



HAL
open science

The Pristine Inner Galaxy Survey (PIGS)

Federico Sestito, Anke Ardern-Arentsen, Sara Vitali, Martin Montelius,
Romain Lucchesi, Kim A Venn, Nicolas F Martin, Julio F Navarro, Else
Starkenbourg

► **To cite this version:**

Federico Sestito, Anke Ardern-Arentsen, Sara Vitali, Martin Montelius, Romain Lucchesi, et al..
The Pristine Inner Galaxy Survey (PIGS). *Astronomy and Astrophysics - A&A*, 2024, 690, pp.A333.
10.1051/0004-6361/202451258 . insu-04757110

HAL Id: insu-04757110

<https://insu.hal.science/insu-04757110v1>

Submitted on 28 Oct 2024

HAL is a multi-disciplinary open access archive for the deposit and dissemination of scientific research documents, whether they are published or not. The documents may come from teaching and research institutions in France or abroad, or from public or private research centers.




L'archive ouverte pluridisciplinaire **HAL**, est destinée au dépôt et à la diffusion de documents scientifiques de niveau recherche, publiés ou non, émanant des établissements d'enseignement et de recherche français ou étrangers, des laboratoires publics ou privés.



Distributed under a Creative Commons Attribution 4.0 International License

The Pristine Inner Galaxy Survey (PIGS)

X. Probing the early chemical evolution of the Sagittarius dwarf galaxy with carbon abundances

Federico Sestito^{1,2,*} , Anke Ardern-Arentsen³, Sara Vitali^{4,5} , Martin Montelius⁶, Romain Lucchesi⁷ ,
Kim A. Venn¹, Nicolas F. Martin^{8,9}, Julio F. Navarro¹, and Else Starkenburg¹⁰

¹ Department of Physics and Astronomy, University of Victoria, PO Box 3055, STN CSC, Victoria BC V8W 3P6, Canada

² Centre for Astrophysics Research, Department of Physics, Astronomy and Mathematics, University of Hertfordshire, Hatfield AL10 9AB, UK

³ Institute of Astronomy, University of Cambridge, Madingley Road, Cambridge CB3 0HA, UK

⁴ Instituto de Estudios Astrofísicos, Universidad Diego Portales, Av. Ejército Libertador 441, Santiago, Chile

⁵ Millennium Nucleus ERIS, Chile

⁶ Kapteyn Astronomical Institute, University of Groningen, Landleven 12, 9747 AD Groningen, The Netherlands

⁷ Dipartimento di Fisica e Astronomia, Università degli Studi di Firenze, Via G. Sansone 1, 50019 Sesto Fiorentino, Italy

⁸ Université de Strasbourg, CNRS, Observatoire astronomique de Strasbourg, UMR 7550, 67000 Strasbourg, France

⁹ Max-Planck-Institut für Astronomie, Königstuhl 17, 69117 Heidelberg, Germany

¹⁰ Kapteyn Astronomical Institute, University of Groningen, Landleven 12, 9747 AD Groningen, The Netherlands

Received 26 June 2024 / Accepted 5 September 2024

ABSTRACT

We aim to constrain the chemo-dynamical properties of the Sagittarius (Sgr) dwarf galaxy using carbon abundances. At low metallicities in particular, these properties reveal the early chemical evolution of a system, tracing the contributing supernovae (SNe) and how much of their ejecta eventually made it into the next stellar generation. Our sample from the Pristine Inner Galaxy Survey (PIGS) includes ~350 metal-poor ($[\text{Fe}/\text{H}] < -1.5$) stars in the main body of Sgr with good quality spectroscopic observations. Our metal-poor Sgr population has a larger velocity dispersion than metal-rich Sgr from the literature, which could be explained by outside-in star formation, extreme Galactic tidal perturbations, and/or the presence of a metal-rich disc and bar + metal-poor halo. The average carbon abundance $[\text{C}/\text{Fe}]$ in Sgr is similar to that of other classical dwarf galaxies (DGs) and consistently lower than in the Milky Way by $\sim 0.2\text{--}0.3$ dex at low metallicities. The interstellar medium in DGs, including Sgr, may have retained yields from more energetic Population III and II supernovae (SNe), thereby reducing the average $[\text{C}/\text{Fe}]$. Additionally, SNe Ia producing more Fe than C would start to contribute at lower metallicity in DGs/Sgr than in the Galaxy. The presence of a $[\text{C}/\text{Fe}]$ gradient for Sgr stars with $[\text{Fe}/\text{H}] \gtrsim -2.0$ ($\sim 6.8 \times 10^{-4}$ dex arcmin⁻¹) suggests that SNe Ia contributed to the system at those metallicities, especially in its inner regions. There is a low frequency of carbon-enhanced metal-poor (CEMP) stars in our Sgr sample. At higher metallicities and carbon abundances (i.e. mostly CEMPs), this may be due to photometric selection effects, but those are less likely to affect non-CEMP stars. Given the lower average $[\text{C}/\text{Fe}]$ in DGs, we propose using the same CEMP definition ($[\text{C}/\text{Fe}] > +0.7$) as that applied to the Galaxy at large ends up underpredicting the number of CEMP stars in DGs. Furthermore, for Sgr, a cut at $[\text{C}/\text{Fe}] \sim +0.35$ may be more appropriate, which brings the frequency of CEMP stars in agreement with that of the whole Galaxy.

Key words. stars: abundances – stars: Population II – galaxies: abundances – galaxies: dwarf – galaxies: individual: Sagittarius

1. Introduction

The Sagittarius (Sgr) dwarf galaxy (Ibata et al. 1994), located approximately 26.5 kpc away from us towards the inner Galactic regions (Vasiliev & Belokurov 2020), experienced its first in-fall into the Milky Way (MW) about 5 Gyr ago (e.g. Ruiz-Lara et al. 2020). As it is in the process of being tidally stripped by the MW, its core and two stellar streams are now visible in the Sky (Ibata et al. 1994; Mateo 1998; Majewski et al. 2003; Law & Majewski 2010; Belokurov et al. 2014), as well as various associated globular clusters (Sbordone et al. 2007; Mucciarelli et al. 2017). Given its proximity, it is an ideal test-bed for galactic chemo-dynamical models.

The star formation history (SFH) of Sgr is characterised by multiple star formation episodes, investigated with both

high-resolution spectroscopy (e.g. Bonifacio et al. 2000; Monaco et al. 2005; Chou et al. 2007; McWilliam et al. 2013; Hansen et al. 2018a; Hasselquist et al. 2017, 2021; Sestito et al. 2024b) and photometric techniques (e.g. Bellazzini et al. 1999; Layden & Sarajedini 2000; Siegel et al. 2007; Vitali et al. 2022). So far, studies have typically focussed on metal-rich and relatively young stars, given that they are the prevalent population. Further complicating the study of the oldest and most metal-poor stars is the strong overlap in the colour-magnitude diagram between the Milky Way bulge population and stars in Sgr (Monaco et al. 2005; Mucciarelli et al. 2017); especially on the blue, metal-poor side of the red giant branch (RGB) of Sgr. However, the most metal-poor stars are key to understanding the early chemical evolution of Sgr.

An efficient way to discover new members in dwarf galaxies is to use the exquisite Gaia (Gaia Collaboration 2016, 2021, 2023) astrometry and photometry alone (e.g. Chiti et al. 2021;

* Corresponding author; f.sestito@herts.ac.uk

Filion & Wyse 2021; Yang et al. 2022; Waller et al. 2023; Sestito et al. 2023a,c; Hayes et al. 2023; Jensen et al. 2024) or to couple it with metal-poor dedicated photometric surveys, such as the Pristine survey (Starkenburg et al. 2017; Martin et al. 2023), as done in the Pristine dwarf galaxy survey (e.g. Longeard et al. 2022, 2023).

Along those lines, the Pristine Inner Galaxy Survey (PIGS) targets metal-poor stars towards the inner regions of the MW (Arentsen et al. 2020b), as well as the Sagittarius dwarf galaxy (Vitali et al. 2022). The latter work investigated the metallicity distribution of $\sim 50\,000$ Sgr candidate members as a function of their spatial location and identified the largest sample of Sgr candidate members with $[\text{Fe}/\text{H}] \leq -2.0$ (~ 1200 stars). From PIGS, Sestito et al. (2024b) followed-up with MIKE high-resolution spectroscopy 12 very metal-poor (VMP, $[\text{Fe}/\text{H}] \leq -2.0$) Sgr members, the largest and most complete detailed chemical abundance analysis of the VMP Sgr component (vs 4 VMPs in Hansen et al. 2018a). The authors interpreted the chemical pattern of the most metal-poor stars as the result of a variety of type II supernovae and asymptotic giant branch stars. A wide range of energetic supernovae and hypernovae with intermediate mass ($10\text{--}70 M_{\odot}$) are needed to account for the chemical abundances of the lighter elements up to the Fe-peak. The chemical trend of the heavier elements is interpreted as a mixture of yields from compact binary mergers and massive (up to $\sim 120 M_{\odot}$) fast-rotating stars (up to $\sim 300 \text{ km s}^{-1}$).

Investigating the origin of carbon in a given stellar population is crucial to understand various astrophysical topics; for example, the types of supernovae contributing in a given system, nucleosynthesis in massive stars, and binary interaction mechanisms (e.g. Frebel et al. 2007; Vincenzo & Kobayashi 2018; Kobayashi et al. 2020). At low metallicity, many stars are found to be carbon-enhanced. Populations of these so-called carbon-enhanced metal-poor (CEMP) stars, with $[\text{C}/\text{Fe}] > +0.7$, are powerful probes of the underlying stellar population and the star formation history. Some CEMP stars are thought to carry the imprint of the first generations of supernovae, these are called CEMP-no stars and have sub-solar Ba, namely, $[\text{Ba}/\text{Fe}] < 0.0$ (Beers & Christlieb 2005; Aoki et al. 2007). It has been suggested that classical DGs have a lower CEMP-no fraction than the MW halo and ultra-faint dwarfs (UFDs) (e.g. Starkenburg et al. 2013; Jablonka et al. 2015; Kirby et al. 2015b; Simon et al. 2015; Hansen et al. 2018b; Lucchesi et al. 2024; Skúladóttir et al. 2015, 2021, 2024b).

Other types of CEMP stars are typically the products of mass transfer from binary interaction with a former asymptotic giant branch (AGB) star companion. These are Ba-rich ($[\text{Ba}/\text{Fe}] > +1.0$) due to slow-process channels taking place in the AGB companion and are called CEMP-s stars (Beers & Christlieb 2005). The latter group is important to understand the properties of binary populations. In particular, their properties are instructive to understand the nucleosynthetic channels, convection and non-convective processes (e.g. Stancliffe et al. 2007); the interaction mechanisms, such as the physics of Roche-lobe overflow and wind accretion (e.g. Abate et al. 2013); and their influence on the measurement of the velocity dispersion in a system and its dynamical mass (e.g. Spencer et al. 2017; Arroyo-Polonio et al. 2023), such as its dark matter content.

From medium-resolution spectroscopy, metallicities and carbon abundances have been measured in only 11 VMP stars in Sgr (Chiti & Frebel 2019; Chiti et al. 2020). In this work, we use the data release of the PIGS low/medium-resolution spectroscopic campaign (Ardern-Arentsen et al. 2024) to select the

largest sample of low-metallicity ($[\text{Fe}/\text{H}] \leq -1.5$) Sgr members (356 stars) with measured metallicity, $[\text{C}/\text{Fe}]$, and radial velocity to date. The dataset and a discussion on the photometric selection effects due to the Pristine filter is reported in Sect. 2. The dynamical properties of the metal-rich and metal-poor populations in Sgr are outlined in Sect. 3. A comparison of the $[\text{C}/\text{Fe}]$ abundances in Sgr with respect the other classical dwarf galaxies (DGs) and the MW halo and inner Galaxy is discussed in Sect. 4. We discuss the types and frequencies of CEMP stars in Sgr in Sect. 5, including a suggestion that the definition of CEMP might need revision in DGs. Our conclusions are summarised in Sect. 6.

2. Pristine Inner Galaxy Survey (PIGS)

PIGS targets the most metal-poor stars in the inner regions of the Milky Way (Arentsen et al. 2020b), using a metallicity-sensitive narrow *CaHK* filter mounted at Canada-France-Hawaii Telescope (CFHT). Among the photometric metal-poor candidates, $\sim 13\,235$ stars have been observed with the Anglo Australian Telescope (AAT) using the AAOmega+2dF spectrograph. We will refer to them as the PIGS/AAT sample, which is publicly available (Ardern-Arentsen et al. 2024). The AAT setup acquired spectra with low-resolution ($R \sim 1800$) in the blue and with medium-resolution ($R \sim 11\,000$) around the calcium triplet. The analysis is described in detail in Arentsen et al. (2020a), but, briefly, the two arms were fit simultaneously with the FERRE code¹ (Allende Prieto et al. 2006) to obtain stellar parameters (effective temperature and surface gravity), metallicities, and carbon abundances. The radial velocities (RVs) were derived by cross-correlation of the calcium triplet spectra with synthetic templates.

2.1. PIGS target selection from photometry

Some of the PIGS/AAT fields overlap with the core of the Sagittarius dwarf galaxy. In four fields, Sgr stars were specifically targeted. Two fields were observed in 2018 and served as a pilot program (Field282.0-29.8_Sag, Field284.0-30.0_Sag), two additional fields with more Sgr candidates were observed in 2020 (Field282.9-32.1, Field286.0-31.1). For the 2018 observations, Sgr stars were selected to be within a radius of 0.6 mas yr^{-1} around proper motions of $\mu_{\alpha} = -2.7 \text{ mas yr}^{-1}$ and $\mu_{\delta} = -1.35 \text{ mas yr}^{-1}$ and parallax_error $< 0.05 \text{ mas}$. This was relaxed slightly in 2020, to a radius of 1 mas yr^{-1} around those proper motions and the parallax_error of $< 0.1 \text{ mas}$. In 2020, suspected variable stars were removed using the flux error and the number of observations (Fernández-Alvar et al. 2021). Both selections were done using Gaia DR2 (Gaia Collaboration 2018).

The photometric calibration of the PIGS *CaHK* photometry was slightly different when the targets were selected compared to the current, final photometric catalogue, but the changes are not expected to be major for the Sgr fields. For the fields from 2018, Sgr candidates were selected using a horizontal line in $(\text{CaHK} - G)_0 - 2.5(\text{BP} - \text{RP})_0$ to select the best ~ 100 Sgr targets per field (and the rest of the AAT fibres were filled with inner Galaxy targets). Observed targets can be seen as black or small coloured points in the Pristine colour-colour diagrams in the left-hand panels of Fig. 1, compared to all Sgr candidates in the fields in grey. A red cut at $(\text{BP} - \text{RP})_0 = 1.7$ was also made. For the fields in 2020, a different strategy was used;

¹ <http://github.com/callendeprieto/ferre>

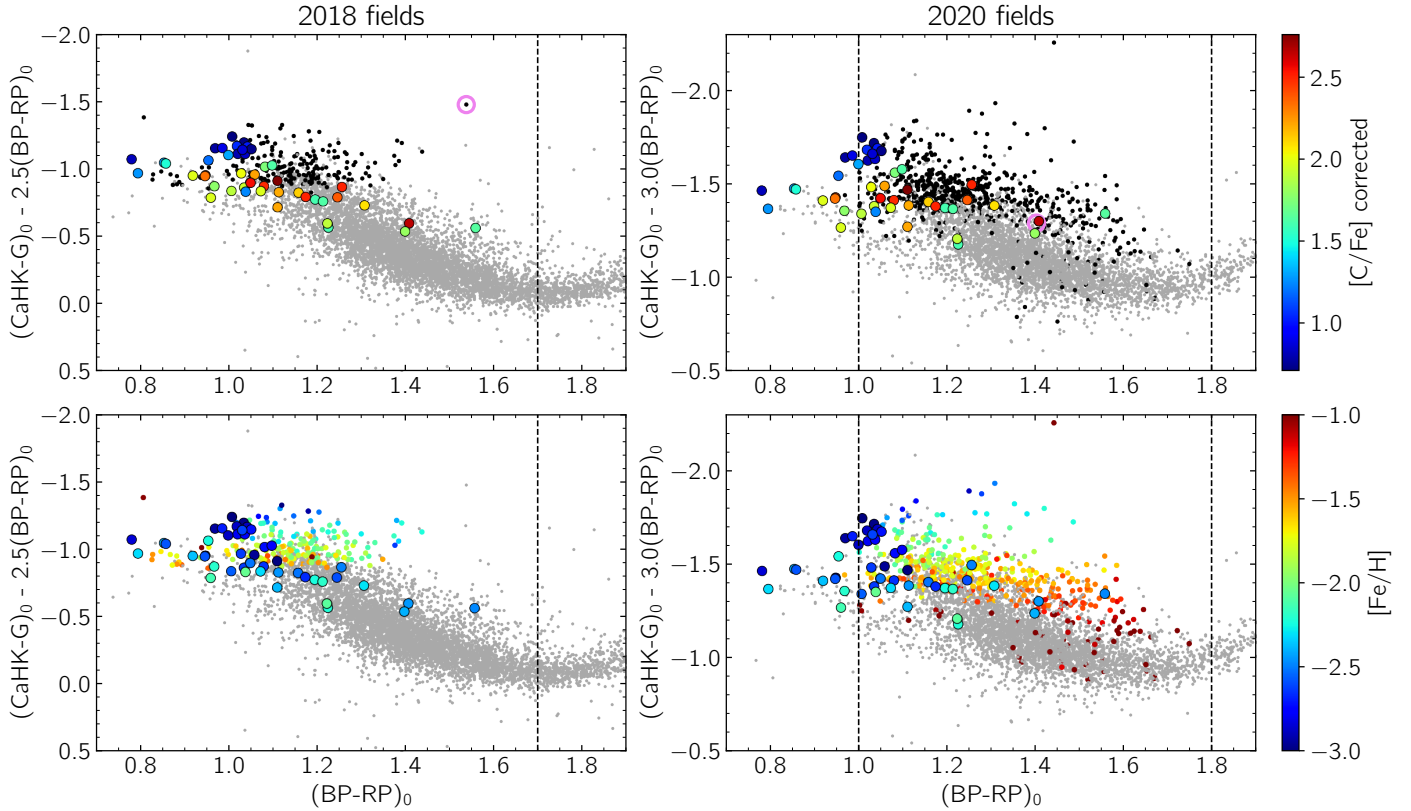


Fig. 1. Colour-colour diagrams for the two fields observed in 2018 (left) and the two observed in 2020 (right). Grey dots are all stars with PIGS photometry in the targeted fields passing the respective Sgr selection criteria for those years (see Sect. 2.1) and $G < 17$. Black dots in the top row are all observed AAT stars in these fields, coloured small dots in the bottom panel are good quality AAT stars coloured by spectroscopic metallicity. Large dots denote Yoon et al. (2016) CEMP stars with $\log g < 2.5$ and $-3 < [\text{Fe}/\text{H}] < -2.0$. Colour coding in the top row is $[\text{C}/\text{Fe}]$, in the bottom is $[\text{Fe}/\text{H}]$. Vertical lines indicate colour cuts applied. The stars within the pink circles in the top left and right panels are discussed in Sect. 5.2 (in the right-hand panel, it is at $(x,y) \sim (1.4, -1.3)$).

namely, the focus was completely on Sgr and inner Galaxy stars were mostly used as fillers if no fibres could be placed on Sgr stars. The Sgr candidates were selected in two ways. The first group contained all stars brighter than $G_0 = 15.5$ and bluer than a $[\text{M}/\text{H}] = -1.0$ MIST isochrone (Choi et al. 2016; Dotter 2016); the aim was to get some red and bright targets that would have been missed in the 2018 selection. The next group contained the most promising metal-poor candidate stars according to *CaHK*, again using a horizontal selection in the colour-colour diagram, this time with factor of 3.0 instead of 2.5 in front of $(\text{BP} - \text{RP})_0$. These selections can be seen as black or small coloured points in the right-hand panels of Fig. 1. A colour cut of $1.0 < (\text{BP} - \text{RP})_0 < 1.8$ was also made.

2.2. Selection effects with reference to CEMP stars

Photometric selections of metal-poor stars are plagued by selection effects against carbon-rich stars, especially for cooler stars (e.g. Beers et al. 1999; Rossi et al. 2005; Goswami et al. 2006; Da Costa et al. 2019; Yoon et al. 2020; Arentsen et al. 2021; Martin et al. 2023). This is because carbon has many molecular features in the spectrum, affecting both the narrow-band and broad-band photometry.

We empirically investigated possible selection effects in our Sgr sample by comparing the location of our observed Sgr/AAT sample in the Pristine colour-colour diagram with known CEMP stars from Yoon et al. (2016, hereafter Y16). We selected giant stars within the relevant Sgr range, making cuts on $\log g < 2.5$

and $-3.0 < [\text{Fe}/\text{H}] < -2.0$. Almost all Y16 stars after this cut have $T_{\text{eff}} > 4500$ K. We used the synthetic *CaHK* catalogue from Martin et al. (2023), derived from Gaia XP spectra (Gaia Collaboration 2023), and cross-matched it with Y16 to obtain Pristine colour-colour diagram positions for these stars. All *CaHK* uncertainties for the Y16 stars are less than 0.075 mag, with more than 80% less than 0.05 mag. For the metal-poor regime in the Sgr/PIGS colour-colour diagrams, the PIGS *CaHK* uncertainties are typically less than 0.025 mag.

The large symbols in Fig. 1 represent CEMP stars from Yoon et al. (2016) in the relevant Sgr range. Unfortunately, the Y16 catalogue does not contain many cool giants in this metallicity range, but a small sample of 48 stars remains that can be used. What is clear is that the CEMP stars are mostly not where they are expected to be, given their metallicity – they are further down in the colour-colour diagrams. A similar conclusion for the Pristine survey was reached by Martin et al. (2023), who reported that these stars have higher photometric metallicities than their spectroscopic metallicities (see also Caffau et al. 2020). Analogously, the SkyMapper survey, which is targeting metal-poor stars with the v filter also in the *CaHK* region, found a similar bias against CEMP stars, especially for those stars with very large carbon-enhancement (predominantly CEMP-s, Da Costa et al. 2019).

For the 2018 fields (left column of Fig. 1), a large fraction of Y16 CEMP stars falls outside the selected region (y -axis ≤ -0.9). These are mostly stars with $[\text{Fe}/\text{H}] > -2.5$ and/or $[\text{C}/\text{Fe}] > +1.8$ – the regime where CEMP-s stars dominate. Stars with

$[\text{Fe}/\text{H}] < -2.5$ and $[\text{C}/\text{Fe}] < +1.8$ fall within the selected range – this combination of $[\text{Fe}/\text{H}]$ and $[\text{C}/\text{Fe}]$ is in the regime of the Group II/CEMP-no stars. In the 2020 fields (right column of Fig. 1), more Sgr stars were targeted and the selection boundary lies slightly lower in the colour-colour diagram. More Y16 CEMP stars now overlap with the selection range, although very much at the edge. The biases are similar to those of the 2018 selection, although a few more stars with $[\text{Fe}/\text{H}] < -2.5$ and $[\text{C}/\text{Fe}] > +2.0$ are included now. From this analysis, we conclude that CEMP-no stars with moderate carbon-enhancement should likely be included in our selection (especially for the 2020 fields, where the majority of our sample comes from), but a large fraction of CEMP-s stars would likely have been excluded.

Finally, we note that the Y16 sample does not have any stars cooler than 4500 K with $[\text{Fe}/\text{H}] < -2.5$ or with $[\text{Fe}/\text{H}] > -2.5$ and $[\text{C}/\text{Fe}] < +1.5$. It is therefore difficult to estimate the biases against these stars, although we expect them to be worse for such cool stars. Our analysis in this work is focused on slightly warmer stars so the details of these stars are not crucial.

2.3. Sagittarius spectroscopic sample used in this work

For the purposes of this work, to remove the MW contamination from the Sgr candidates, a selection of the Sgr members was made on the basis of the Gaia DR3 proper motions, position on the sky, and radial velocity. In particular, we use the reduced proper motions for Sgr², as defined in Vasiliev & Belokurov (2020). This takes into account that the proper motion of the members changes as a function of the coordinates. We assume a star to be a Sgr member if it exhibits a reduced proper motion of less than 0.6 mas yr⁻¹ as in Vasiliev & Belokurov (2020) and Vitali et al. (2022). Additionally, Sgr members have RVs in the range from 100 to 200 km s⁻¹ (e.g. Ibata et al. 1994; Bellazzini et al. 2008; Minelli et al. 2023). Finally, we limited our analysis to stars with RA > 280°. This leads to a sample of 834 kinematically selected PIGS/AAT Sgr stars.

Not all the AAT spectra have enough good quality to obtain reliable measurements of $[\text{Fe}/\text{H}]$ and $[\text{C}/\text{Fe}]$. Therefore, bad measurements are removed from the kinematical selection using the flag `good_ferre = True`, as suggested in Arden-Arentsen et al. (2024). This flag is based on the S/N of the blue spectra, the FERRE χ^2 and the CaT not being double-lined. This further cut leads to 631 Sgr members with available chemistry. The stars with bad S/N in the AAT sample are partly due to issues with the 2dF fibre placement (see discussion in Arden-Arentsen et al. 2020a), which were particularly severe for the two fields observed in 2020; this is why the upper/right parts of these fields in RA/Dec (see top-left panel of Fig. 2) do not have many stars in the final Sgr cut.

The stellar parameter grid used in FERRE was limited to $4500 \leq T_{\text{eff}}(\text{K}) \leq 7000$ and $1 \leq \log g \leq 5$, implying that for stars at the edge of this grid, an erroneous model atmosphere might have been adopted to derive the $[\text{Fe}/\text{H}]$ and $[\text{C}/\text{Fe}]$. For the Sgr stars, this is particularly problematic at the cool end (see the bottom right panel of Fig. 2); therefore, we removed stars with $T_{\text{eff}} < 4510$ K to avoid stars close to the cool limit of the FERRE grid. For warm stars, the $[\text{C}/\text{Fe}]$ abundances may not be reliable; therefore, we removed stars with $T_{\text{eff}} > 5700$ K. Because we are interested in the chemistry, we only kept the stars with reasonable

² $\mu_\alpha - \bar{\mu}_\alpha = \mu_\alpha + 2.69 - 0.009\Delta\alpha + 0.002\Delta\delta + 0.00002\Delta\alpha^3$,

$\mu_\delta - \bar{\mu}_\delta = \mu_\delta + 1.35 + 0.024\Delta\alpha + 0.019\Delta\delta + 0.00002\Delta\alpha^3$,

where $\Delta\alpha$, $\Delta\delta$ are differences in RA and Dec of each star from the centre of the system ($\alpha_0 = 283.764$ deg, $\delta_0 = -30.480$ deg).

uncertainties on $[\text{Fe}/\text{H}]$ and $[\text{C}/\text{Fe}]$ (<0.5 dex). After these cuts, the PIGS/AAT Sgr sample consists of 437 stars. However, in this work, we are mainly interested in stars with $[\text{Fe}/\text{H}] < -1.5$, which results in a final selection of 356 metal-poor PIGS/AAT Sgr members with good measurements of $[\text{Fe}/\text{H}]$, $[\text{C}/\text{Fe}]$, and RV. A table of the Sgr members updated to Gaia DR3 is available at the CDS.

The PIGS/AAT sample (13 235 stars, grey dots), the stars from the kinematical cut (834, coral circles), the final selection (356 stars, blue circles), and Sgr members from APOGEE DR17 (525 stars, brown crosses, Abdurro'uf et al. 2022) are shown in Fig. 2. The figure displays the position on the sky zoomed in on the Sgr fields (top left panel), the reduced proper motion space (top right), the $[\text{Fe}/\text{H}]$ –RV space (bottom-left), and the Kiel diagram (bottom-right). PIGS/AAT stars in grey dots that lie within the red circle in proper motion space (top-right) do not have RV compatible with Sgr, and, similarly, PIGS/AAT stars in grey dots with similar RV as Sgr (bottom left) do not match its proper motion. The Kiel diagram clearly shows an overdensity of stars at the cool edge of the FERRE grid, which has been removed as outlined above. Most PIGS/AAT Sgr stars have $1.0 < \log g < 2.5$ and $4500 \text{ K} < T_{\text{eff}} < 5300 \text{ K}$.

Part of this work is focused on very carbon-rich objects (Sect. 5), so it is important to be certain that our spectroscopic quality cuts do not bias against such stars. The main quality cuts of relevance are the S/N and the FERRE χ^2 . The S/N is determined from the spectra independently of the FERRE fit, in two regions (4000–4100 Å and 5000–5100 Å), and is not expected to be strongly affected by the carbon abundance, so cutting on it is unlikely to introduce a bias against CEMP stars. If FERRE cannot find a good fit or there are many bad regions in the spectrum, the χ^2 will be high. We inspect all fits of Sgr candidates with bad S/N or bad χ^2 by eye, and identify two clearly carbon-rich stars that are badly fitted, with a high χ^2 . Both of these are very cool, very carbon-enhanced, and intermediate and very metal-poor. They are discussed further in Sect. 5.2.

3. Exploring the RV distribution

The RVs of the PIGS/AAT Sgr sample fall within the overall distribution of stars in Sgr's core, ranging between 100 and 200 km s⁻¹ (e.g. Ibata et al. 1994; Bellazzini et al. 2008; Minelli et al. 2023, see also our Fig. 2). Various studies have pointed out that the metal-poor population of Sgr, both in the core and in the stream, is more spatially extended and has a larger velocity dispersion, σ_{RV} , and a higher systemic velocity, $\langle \text{RV} \rangle$, than the more metal-rich population (e.g. Gibbons et al. 2017; Johnson et al. 2020; Peñarrubia & Petersen 2021; Vitali et al. 2022; Limberg et al. 2023; Minelli et al. 2023). With the PIGS/AAT Sgr sample, we were able to update these quantities using a more metal-poor, and likely older, population than previous work.

The Sgr stars were divided into two populations, the metal-poor ($[\text{Fe}/\text{H}] < -1.5$) from PIGS/AAT and the metal-rich ($[\text{Fe}/\text{H}] > -0.6$) from APOGEE DR17. The number of stars in these two populations as a function of the projected elliptical distance from Sgr's centre is shown in Fig. 3. The metal-rich population dominates over the metal-poor one in the very inner regions, until a projected elliptical distance of ~ 0.25 half-light radii (r_h); at that point, the two groups from the two surveys are similarly populated.

The metal-poor and the metal-rich populations are then divided into two sub-groups according to their projected elliptical distances: the inner group at $<0.25 r_h$ vs. the outer at $\geq 0.25 r_h$.

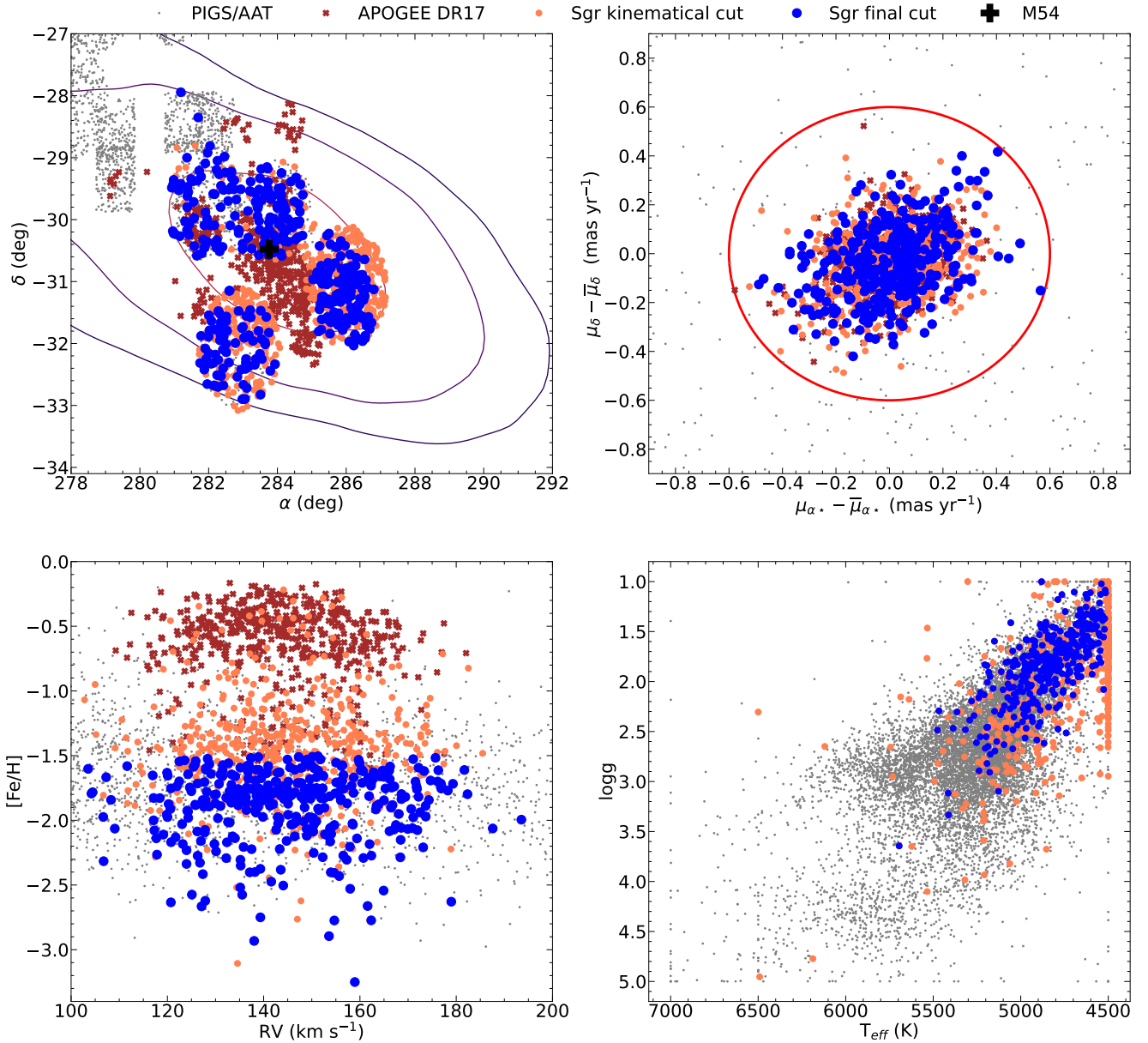


Fig. 2. On-sky position (top-left). Black plus symbols mark the position of the M54 star cluster. Contour lines represent the distribution of Gaia DR3 Sgr candidate members selected on their proper motions as in our kinematical cut. Contour lines mark the position at which the number of Sgr candidate members decreases by a factor of 2, 4, and 6, respectively. Top right panel: reduced proper motion space. Bottom-left: metallicity-radial velocity distribution. Bottom right: Kiel diagram of the PIGS/AAT data, including the Inner Galaxy and Sgr. Blue circles mark the final Sgr cut (356 stars), coral circles denote the Sgr stars from the kinematical selection (834 stars), brown crosses indicate the Sgr members selected from APOGEE DR17, and the grey dots correspond to the PIGS/AAT sample of the inner Galaxy. Sgr members from APOGEE DR17 were selected by imposing a similar RV and proper motion cut as that applied to our sample, along with a high signal-to-noise ratio in the spectra (> 70) to ensure the good quality of the RV and $[Fe/H]$. The APOGEE DR17 stars are not displayed in the Kiel diagram to better highlight the PIGS data.

To derive the systemic RV and the RV dispersion, a Bayesian framework embedded in a Monte Carlo Markov chain, based on the Metropolis-Hastings algorithm, is employed. The prior probability distribution is a step function and it expects these quantities to be in the ranges $90 \leq RV \leq 220$ km s $^{-1}$ and $\sigma_{RV} \leq 40$ km s $^{-1}$. The likelihood is a Gaussian distribution centred on the systemic RV and with a dispersion that takes into account the intrinsic RV dispersion of the system and the uncertainties of the RV measurements. The systemic RV, $\langle RV \rangle$, vs velocity dispersion, σ_{RV} , are displayed in Fig. 4 and reported in Table 1. As reference, Fig. 4 also displays the values for the populations from Minelli et al. (2023), for metal-rich stars ($[Fe/H] > -0.6$, blue

small circle) and metal-poor stars ($[Fe/H] \leq -0.6$, but almost no stars with $[Fe/H] < -1.0$, black small circle). We checked for possible systematics between the APOGEE and PIGS radial velocities by comparing both surveys to Gaia radial velocities (not limited to Sgr to have many more stars). The difference $\Delta RV(\text{PIGS} - \text{Gaia}) = +0.5$ km s $^{-1}$ (Ardern-Arentsen et al. 2024) and $\Delta RV(\text{APOGEE} - \text{Gaia}) = +0.2$ km s $^{-1}$, implying there is only a ~ 0.3 km s $^{-1}$ systematic difference between APOGEE and PIGS.

The overall metal-poor (large blue circle) and metal-rich (large black circle) populations have a systemic RV of 145.4 ± 0.9 km s $^{-1}$ and of $\sim 142.6 \pm 0.7$ km s $^{-1}$, respectively.

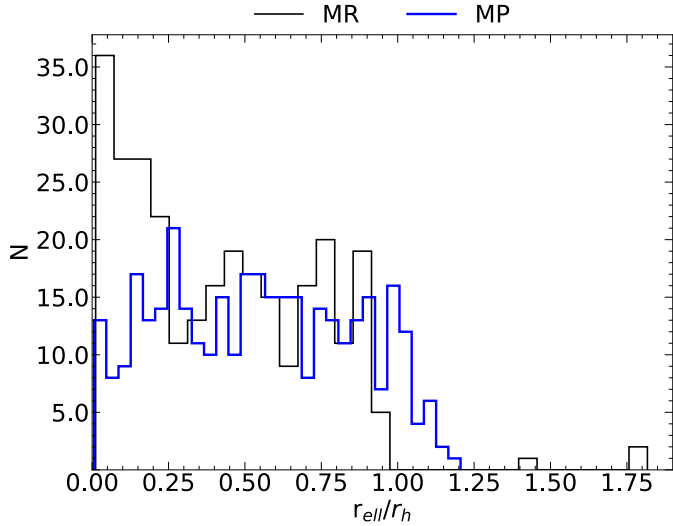


Fig. 3. Number of stars as a function of the projected elliptical distance. The metal-poor ($[\text{Fe}/\text{H}] < -1.5$) and metal-rich ($[\text{Fe}/\text{H}] > -0.6$) are denoted by the blue and black line, respectively. Right ascensions and declinations are converted to tangential plane coordinate assuming the centre of the system as $\alpha_0 = 283.764$ deg and $\delta_0 = -30.480$ deg. The half-light radius is assumed to be 2.6 kpc (Majewski et al. 2003; Mucciarelli et al. 2017) at a distance of 26.5 kpc (Vasiliev & Belokurov 2020), ellipticity ~ 0.57 and position angle ~ -104 deg as in Vitali et al. (2022).

These values are compatible with the ones inferred by Minelli et al. (2023, small circles) adopting a different cut in $[\text{Fe}/\text{H}]$ and a different dataset. The difference in the systemic RV between these populations is significant, given the uncertainties and the precision of the RVs. We did not take into account any projection effects.

Recently, An et al. (2024) modelled the RV distributions of Sgr and M54, and inferred a difference of 4 km s^{-1} between M54 (magenta cross marker) and the main body of Sgr (magenta small circle), with mean radial velocities of $139.6 \pm 0.9 \text{ km s}^{-1}$ for M54 and $143.7 \pm 0.7 \text{ km s}^{-1}$ for the main body, with a velocity gradient in the main body. While our sample does not include stars from M54, our estimate of the systemic velocity for the main body is $144.1 \pm 0.5 \text{ km s}^{-1}$ (magenta large circle), which is compatible with the value from An et al. (2024). Our results suggest that there is additionally a difference between MP and MR Sgr field populations – there appears to be an increasing mean RV going from M54, to metal-rich field stars, to metal-poor field stars.

In agreement with previous work on the stream and core (e.g. Gibbons et al. 2017; Johnson et al. 2020; Peñarrubia & Petersen 2021; Vitali et al. 2022; Limberg et al. 2023; Minelli et al. 2023), we find that the overall metal-poor population has a velocity dispersion larger than the metal-rich counterpart, in our case $\sigma_{\text{RV}} \sim 17 \text{ km s}^{-1}$ vs. $\sigma_{\text{RV}} \sim 12 \text{ km s}^{-1}$, respectively. Also to be noted from Fig. 4: the inner populations in our analysis (large squares), both MP and MR, have lower RV dispersion and lower systemic RV than their respective outer populations (large plus markers). For all the populations and subgroups, the velocity dispersion and the systemic velocity are found to be considerably higher than the values for M54 (magenta cross marker). The latter has been classified as a nuclear star cluster, which might explain its higher velocity dispersion compared to isolated globular clusters. Its velocity dispersion might have been inflated by

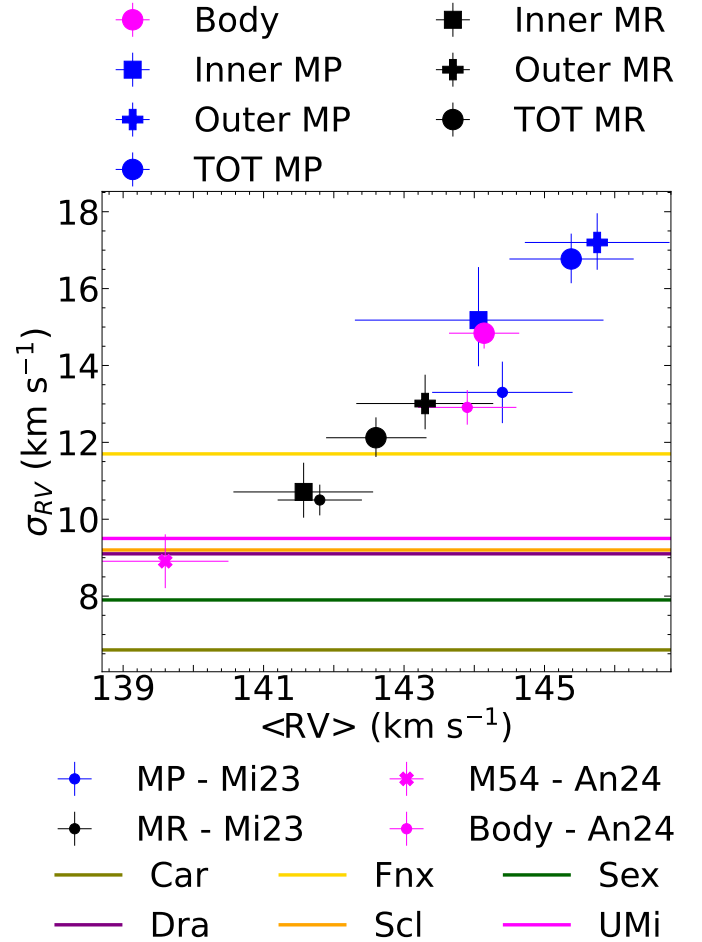


Fig. 4. RV dispersion vs. systemic RV. Large blue and black markers denote the metal-poor ($[\text{Fe}/\text{H}] \leq -1.5$, MP) stars from Sgr/AAT and the metal-rich Sgr population ($[\text{Fe}/\text{H}] > -0.6$, MR) from APOGEE DR17, respectively. The large magenta circle marks the position of the main Sgr's body in this space, considering data from APOGEE and Sgr/AAT. Squares, pluses, and circles correspond to the inner (projected distance $< 0.25r_h$), the outer ($\geq 0.25r_h$), and the whole population, respectively. A systematic error of 2 km s^{-1} is added in quadrature to the RV uncertainties of Sgr/AAT data. The blue and black small circles mark the MP ($[\text{Fe}/\text{H}] \leq -0.6$) and MR ($[\text{Fe}/\text{H}] > -0.6$) populations of Sgr from Minelli et al. (2023), respectively. Magenta cross and small circle denote M54 and the main body of Sgr as measured by An et al. (2024). Horizontal solid lines indicate the RV dispersion of the other classical DGs (McConnachie & Venn 2020).

the dark matter halo of Sgr, by tidal interactions, and by the multiple burst of star formation (e.g. Carlberg & Grillmair 2022; Kacharov et al. 2022; Herlan et al. 2023; Gray et al. 2024). The MP and MR populations should not be contaminated by many M54 members.

3.1. Internal and external mechanisms at play

Various internal and external mechanisms can affect the chemodynamical properties of a system. For instance, the internal morphology can play a role. In this regard, a dynamically hotter MP and a colder MR population with weak rotation has been proposed to indicate the presence of a metal-rich thick and rotating disc or bar surrounded by a more dispersed and metal-poor stellar halo in Sgr (Mayer et al. 2001; Sánchez-Janssen et al. 2010;

Table 1. Systemic RV and RV dispersions.

Population	$\langle \text{RV} \rangle$ (km s^{-1})	σ_{RV} (km s^{-1})	Dataset
MR–Inner	$141.6^{+1.0}_{-1.0}$	$10.7^{+0.8}_{-0.7}$	APOGEE
MR–Outer	$143.3^{+1.0}_{-1.0}$	$13.0^{+0.8}_{-0.7}$	APOGEE
MR–Tot	$142.6^{+0.7}_{-0.7}$	$12.1^{+0.5}_{-0.5}$	APOGEE
MP–Inner	$144.1^{+1.8}_{-1.8}$	$15.2^{+1.4}_{-1.2}$	AAT
MP–Outer	$145.8^{+1.0}_{-1.0}$	$17.2^{+0.8}_{-0.7}$	AAT
MP–Tot	$145.4^{+0.9}_{-0.9}$	$16.8^{+0.7}_{-0.6}$	AAT
Body	$144.1^{+0.5}_{-0.5}$	$14.8^{+0.4}_{-0.4}$	AAT + APOGEE

Notes. Systemic RVs and RVs dispersions for the metal-poor and metal-rich populations and for the whole body. The values for the inner, outer, and whole groups are reported, together with the source of the datasets.

Kazantzidis et al. 2011; del Pino et al. 2021; Carlberg & Grillmair 2022; Minelli et al. 2023; Lokas 2024). Both observations and simulations suggest that the rotating bar should have a length of 2–2.5 kpc (del Pino et al. 2021; Lokas 2024), which correspond to an elliptical radius of 0.8–1.0 r_{h} . As shown in Fig. 3, the majority of the stars from both APOGEE and PIGS lies within 1 half-light radius. The presence of such a rotating disc or bar would also explain some chemo-dynamical properties of the stellar streams associated with Sgr (Peñarrubia et al. 2010; Orlia et al. 2022; Carlberg & Grillmair 2022). The fact that the MR population, either in the inner or outer regions, has a lower velocity dispersion and a lower systemic RV than the MP supports the idea that these two groups populate two different structures, such as a ‘disc and bar’ and a stellar ‘halo’ for Sgr. If so, projection effects on the bar are another ingredient explaining the different systemic RV from the MP group.

Additionally, outside-in star formation has been proposed as one mechanism to explain the different spatial and kinematical properties between MP and MR populations in DGs, such as the gradient in the velocity dispersion (e.g. Tolstoy et al. 2004; Battaglia et al. 2006, 2008; Zhang et al. 2012; Hidalgo et al. 2013; Benítez-Llambay et al. 2016; Revaz & Jablonka 2018; Sestito et al. 2023a,c; Tolstoy et al. 2023). In this scenario, the oldest MP population would form spatially everywhere in the system, and their supernovae would enrich the ISM. Then some of the gas might have sunk to the inner region with time, forming younger and more metal-rich stars that are more gravitationally bound to the system. As a result of this, the MP population would be more spatially extended and kinematically hotter than the MR one, with the latter being confined mostly to the inner regions with a lower velocity dispersion.

The main external mechanisms that can affect the dynamical properties of a DG are merging events and tidal stripping. In case of the former, stars will be heated up by the accreted system, and likely the less bound ones, such as in the outskirts, will be more affected. Then, the additional gas from the accreted system (if it has any) can sink into the inner regions, triggering the formation of new stars that are more metal-rich (Benítez-Llambay et al. 2016). In addition, tidal stripping also influences the distribution and kinematics of the outskirts, which are less bound, of a system. In fact, the ongoing stripping of Sgr resulted

in the formation of the Sgr stellar streams, which are known to be more metal-poor on average than the core (e.g. Hayes et al. 2020; Limberg et al. 2023; Cunningham et al. 2024). It has been proposed that Sgr has interacted gravitationally with the MW for more than 8 Gyr, with its first pericentric passage likely to have happened around 5–6 Gyr ago (Law & Majewski 2010; Ruiz-Lara et al. 2020). The MR population in Sgr has an estimated age spanning from 4 to 8 Gyr – their star formation, or part of it, might have been triggered by Galactic perturbations at, or close to, the first pericentric passage. Investigations on simulated galaxies reveals that the extreme tidal effects that Sgr is undergoing might have affected the system’s morphology, e.g. it could have reshaped its disc (if it had one) into a prolate rotating bar structure (Lokas 2024).

3.2. Comparison to other DGs

The values of the velocity dispersion for the other 6 classical DGs (horizontal lines, McConnachie & Venn 2020) are also reported in Fig. 4 as a reference. The velocity dispersion for the MR population in Sgr is similar to Fornax’s value, which is the highest among the DGs compilation. The σ_{RV} for the MP population in Sgr is significantly higher than the averages for the other DGs. This could be due to an observational bias, such as the σ_{RV} in the reference galaxies are calculated from the overall population, which is mostly more metal-rich than the MP population in Sgr. As an example, the velocity dispersion for the overall population in Sculptor is around 7 km s^{-1} , while restricting to the more dispersed metal-poor stars would provide a $\sigma_{\text{RV}} \sim 10\text{--}12 \text{ km s}^{-1}$ (Tolstoy et al. 2004; Battaglia et al. 2008; Walker & Peñarrubia 2011; Tolstoy et al. 2023; Sestito et al. 2023a). In addition, Sgr has a total mass higher than the other DGs reported in Fig. 4 and it is experiencing strong Galactic tidal stripping, which is far more extreme than in the other systems (e.g. Battaglia et al. 2022; Pace et al. 2022, and references therein), which both concur to inflate the σ_{RV} of this system.

4. Carbon trends in Sagittarius

We next focus our attention on the chemistry of Sgr and, specifically, the abundance of carbon. As discussed in the introduction, carbon abundances can trace the early chemical evolution of a system (e.g. Frebel et al. 2007; Vincenzo & Kobayashi 2018; Kobayashi et al. 2020). Is the level of carbon in Sgr similar to that in the other classical DGs? What about in comparison with the inner Galaxy and the MW halo? To answer these questions, in Fig. 5 we present the average [C/Fe] ratio as a function of the metallicity for Sgr (red circles) compared to the classical DGs (left panel) and compared to the inner Galaxy and the MW halo (right panel). All carbon abundances have been corrected for evolutionary effects according to Placco et al. (2014), see Arentsen et al. (2021) for details. We find that the Sgr carbon abundance slightly rises with decreasing metallicity.

4.1. Halo and inner Milky Way

There are a number of studies that have explored the carbon abundance of low-metallicity stars in the MW halo, and to a lesser extent in the inner Galaxy. Arentsen et al. (2022) showed that trends involving carbon abundances are very sensitive to the assumptions made in the synthetic spectroscopic grids (e.g. the model atmospheres, the adopted atomic and molecular data) and the employed pipeline, with large systematic offsets between

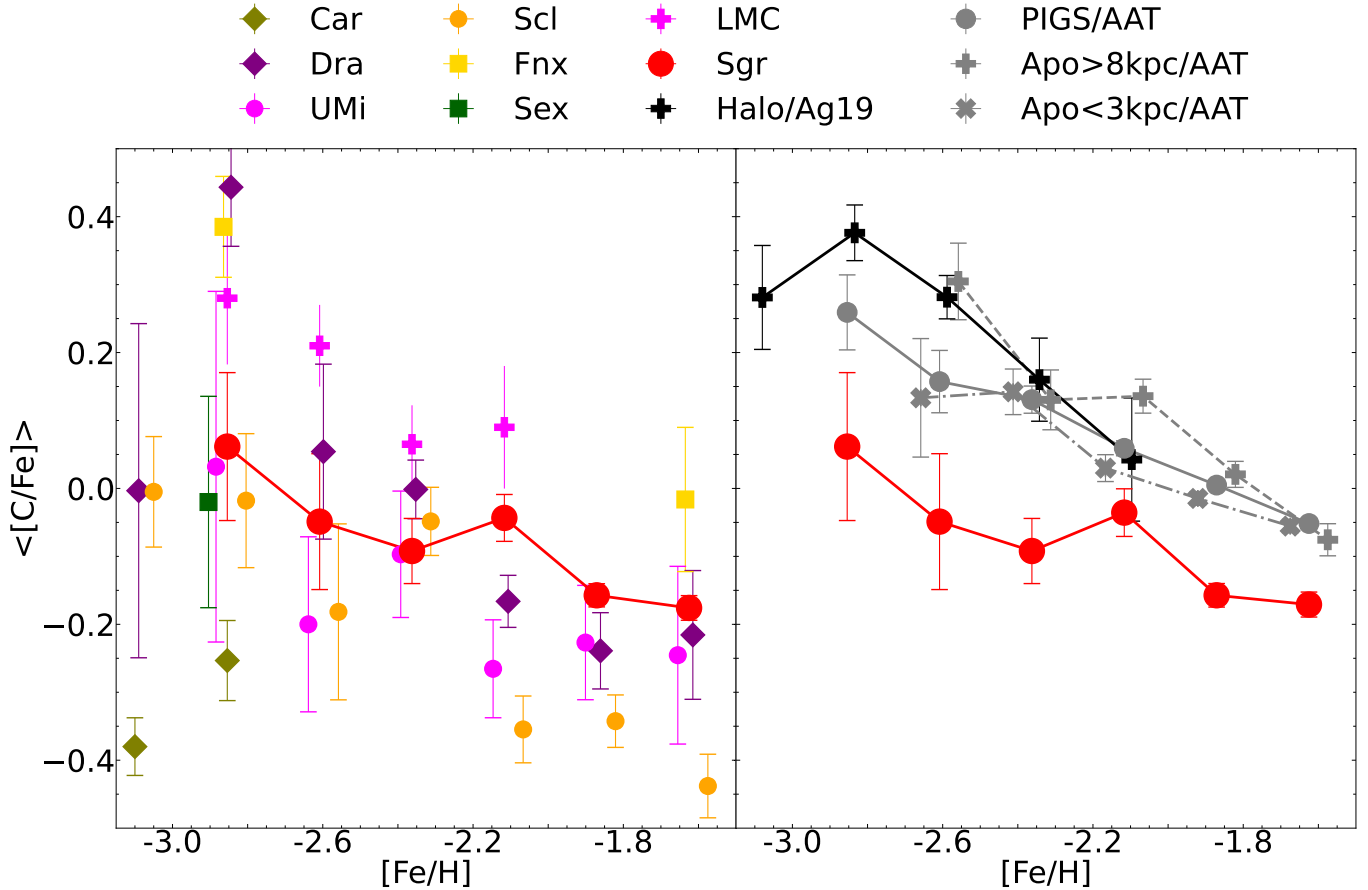


Fig. 5. Average $[C/Fe]$ vs. $[Fe/H]$ divided into seven metallicity bins (~ 0.25 dex). CEMP stars have been removed and carbon abundances have been corrected for evolutionary effects according to [Placco et al. \(2014\)](#). Left panel: comparison with classical DGs (coloured markers), Car, Dra, Fnx, Scl, Sex, and Umi are from [Lucchesi et al. \(2024\)](#), while LMC data is from [Chiti et al. \(2024\)](#) and [Oh et al. \(2024\)](#). $[C/Fe]$ in classical DGs for which there are less than two stars are not displayed. Right panel: comparison with the MW. MW halo stars (black markers) are from [Aguado et al. \(2019\)](#), revised as in [Arentsen et al. \(2022\)](#). Inner Galaxy from PIGS/AAT (grey markers, [Ardern-Arentsen et al. 2024](#)) are divided into three groups, the whole sample (grey circles, solid line), the stars confined into the inner regions (grey crosses, dash-dot line, apocenter < 3 kpc) and the halo interlopers (grey plusses, dash-line, apocenter > 8 kpc). Bins populated by less than five stars have been removed. MW stars from PIGS are selected to have $\log g < 2.3$, while compilation from [Aguado et al. \(2019\)](#) is restricted to stars with $\log g < 3.0$. In both cases, AGBs are removed. $[C/Fe]$ ratios from all the datasets are corrected for the evolutionary effects as in [Placco et al. \(2014\)](#). An offset of up to ± 0.05 is added to the metallicity bins of the MW and DGs compilations to better display the markers and the uncertainties on the average $[C/Fe]$.

different literature samples (see their Fig. 4). To avoid biasing our conclusions, in the comparison with the halo and the inner Galaxy, we restrict ourselves to $[C/Fe]$ measured within PIGS and the Pristine survey, which have all been derived with the same methodology.

The inner Galaxy PIGS/AAT sample was selected from [Ardern-Arentsen et al. \(2024\)](#) and restricted to those stars with good measurements of stellar parameters, metallicities and carbon abundances, as in our Sgr sample. An additional cut was imposed to select stars with similar surface gravity as the bulk of the Sgr sample ($\log g < 2.3$) and to remove the region of early asymptotic giant branch stars (eAGBs) whose carbon abundances have been altered by stellar evolution ([Arentsen et al. 2021](#)). This selection is composed of 2318 stars with $[Fe/H] < -1.5$ (grey circles in the right-hand panel of Fig. 5). Additionally, this sample is split into two sub-groups according to their Galactic apocentric distances, those that remain confined in the inner Galaxy (apocentre < 3 kpc, grey crosses) and the ‘halo interlopers’ (apocentre > 8 kpc, grey plus markers). The former and the latter are composed of 1032 and 276 stars, respectively. For the MW halo, we include the Pristine medium-resolution follow-up

sample from [Aguado et al. \(2019\)](#), 141 stars, black plus markers), with carbon abundances corrected for spurious $\log g$ determinations following [Arentsen et al. \(2022\)](#). This sample has a less restrictive cut on the surface gravity, namely $\log g < 3.0$.

Although the same trend is visible for the Milky Way and Sgr samples, namely, a rise in carbon abundance with decreasing metallicity, the average carbon abundances are higher in the Milky Way samples compared to Sgr, and the rise appears to be less steep in Sgr. The $[C/Fe]$ difference between Sgr and the Milky Way starts at ~ 0.1 dex for $[Fe/H] = -1.6$ and increases to $0.3\text{--}0.4$ dex for $[Fe/H] < -2.5$.

The average carbon abundance of the MW (inner regions and the halo) is also higher than most of the classical DGs, except for Fornax (Fnx, gold squares). The difference in carbon abundances can be interpreted as a different population of SNe II and AGB stars that contributed to the chemical enrichment of the dwarf galaxies in comparison with the one of the Galaxy. In particular, a higher contribution of faint and core-collapse SNe could provide a higher $[C/Fe]$ ratio ([Umeda & Nomoto 2003](#); [Limongi & Chieffi 2003](#); [Iwamoto et al. 2005](#); [Kobayashi et al. 2006, 2020](#); [Vanni et al. 2023](#)).

The physical and chemical properties of the building blocks that contributed to the formation of the proto-Galaxy are still under discussion (e.g. Schiavon et al. 2017; Helmi 2020; Santistevan et al. 2021; Sestito et al. 2021), as well as the importance of an ancient in-situ component (Belokurov & Kravtsov 2022, 2023). Did the early building blocks have a chemical evolution similar of the present UFDs? What about their masses and sizes, or, in other words, are the building blocks comparable to classical DGs or to smaller UFDs (see Deason et al. 2016)?

For the PIGS inner Galaxy sample, there is a slight difference in the average level of carbon abundance between the ‘confined’ (plus symbols, lower [C/Fe]) and ‘halo interloper’ (crosses, higher [C/Fe]) samples, of the order of 0.05–0.10 dex. This could potentially be connected to different building blocks contributing to these populations, for instance, more chemically evolved ones to the confined population and more chemically pristine systems to the halo population (also see the discussion in Ardern-Arentsen et al. 2024). We further discuss the connection to dwarf galaxies and their chemical evolution in Sect. 4.3.

4.2. Note on possible systematics

As previously discussed, the PIGS/AAT inner Galaxy and the Sgr stars have been analysed with the same methodology applied to the same AAT spectra, and the Aguado et al. (2019) sample has been analysed with the same methodology as well, so systematic differences should hopefully be minimal. One caveat here is that $[\alpha/\text{Fe}]$ is fixed in the analysis, to +0.4. However, various high-resolution spectroscopic works showed that the majority of the inner Galaxy VMP stars have similar $[\alpha/\text{Fe}]$ compared to typical halo stars (Howes et al. 2014, 2015, 2016; Sestito et al. 2023b) and the α -abundances are also very similar between the MW and Sgr in the VMP regime (Hansen et al. 2018a; Sestito et al. 2024b). Therefore, we should not expect significant biases in the FERRE analyses due to $[\alpha/\text{Fe}]$ differences.

We note that the magnitude of the evolutionary carbon correction following Placco et al. (2014) also depends on the natal nitrogen abundances of stars, which may differ for each formation site, but are all assumed to be $[\text{N}/\text{Fe}] = 0.0$ in the calculations. However, the predicted effect on the carbon corrections is much smaller than the difference we find between Sgr and the Milky Way – Figure 1 of Placco et al. (2014) shows that for a $[\text{Fe}/\text{H}] = -2.3$ star, the difference in the carbon correction between a $[\text{N}/\text{Fe}]$ of -0.5 and $+0.5$ at birth is at most ~ 0.05 dex. Therefore, a different average level of $[\text{N}/\text{Fe}]$ between the MW and Sgr would not impact our findings. The evolutionary corrections may also potentially be better or worse in some parts of the parameter space (e.g. depending on $\log g$), so it is crucial to compare stars in similar evolutionary phases. We attempted this by limiting the reference samples in $\log g$, but the distributions of evolutionary phases are not exactly the same.

We considered what the effect of photometric selection effects on trends of carbon might be. As discussed previously, very carbon-rich stars were likely excluded from our selection because they appeared ‘too metal-rich’. We considered whether our selection could be biased even for ‘carbon-normal’ stars, restricted only to those with relatively lower carbon abundances. We find that this is unlikely to be the case, especially for $[\text{Fe}/\text{H}] < -2$, given that the carbon features are relatively weak for carbon-normal VMP stars and given that our selection was not only targeting VMP stars, but also probed the slightly more metal-rich population.

Finally, we checked the potential systematics on the mean [C/Fe] and its trend with metallicity as a function of the surface gravity. As a sanity check, we repeated the exercise of Fig. 5, restricting the Sgr and MW compilations to stars with $1.8 < \log g < 2.3$ (for lower $\log g$, the Placco et al. 2014 evolutionary carbon corrections become more important). We find no qualitative or quantitative differences between this more strict cut and the one applied to produce Fig. 5. However, we note that the MW halo sample from Aguado et al. (2019) would not contain enough stars to populate all the metallicity bins for this limited $\log g$ selection.

4.3. Dwarf galaxies

To compare the average [C/Fe] of Sgr with classical DGs, stars with $[\text{Fe}/\text{H}] \leq -1.5$ were selected from the DG members summarised in Lucchesi et al. (2024), Chiti et al. (2024), and Oh et al. (2024). The compilation from Lucchesi et al. (2024) is composed of 442 stars (16 CEMP-no) and distributed throughout classical DGs, namely Canes Venatici I (CVn I, 1 star, Yoon et al. 2020), Carina (Car, 8 stars, Venn et al. 2012; Susmitha et al. 2017; Lucchesi et al. 2024), Draco (Dra, 161 stars, Kirby et al. 2015a), Fornax (Fnx, 14 stars, Tafelmeyer et al. 2010; Kirby et al. 2015a; Lucchesi et al. 2024), Sculptor (Scl, 173 stars, Kirby & Cohen 2012; Kirby et al. 2015a; Skúladóttir et al. 2015, 2024b), Sextans (Sex, 4 stars, Tafelmeyer et al. 2010; Lucchesi et al. 2020), and Ursa Minor (UMi, 81 stars, Kirby & Cohen 2012; Kirby et al. 2015a). The compilations from Chiti et al. (2024) and Oh et al. (2024) include members of the Large Magellanic Cloud (LMC) for a total of 21 stars (no CEMP). The systems from these compilations, excluding CVn I and CEMP-no stars, are displayed in Fig. 5 with coloured circles, diamonds, squares, and plusses.

The average level of [C/Fe] in Sgr is within the wide range of the seven classical DGs. In particular, the average carbon abundance in Sgr appears to be higher than in Scl for $[\text{Fe}/\text{H}] > -2.4$ by up to ~ 0.3 dex. Compared to Car, Sgr’s [C/Fe] level is also higher, for $[\text{Fe}/\text{H}] \leq -2.4$ by at least ~ 0.3 dex. As proposed by Skúladóttir et al. (2024b), the strikingly low amount of [C/Fe] in Scl and Car might be explained by a strong imprint of hypernovae from Pop III stars. Thus, classical DGs and stars with such a low carbon level might be crucial for improving our understanding of the energy distribution of the primordial generation of stars (e.g. Koutsouridou et al. 2023).

Another nucleosynthetic channel that contributes to lower the [C/Fe] is from SNe Ia, in which the production of Fe exceeds that of C (Iwamoto et al. 1999). This event might be responsible for lowering the [C/Fe] in Dra and UMi for $[\text{Fe}/\text{H}] \gtrsim -2.5$, as also shown in Kirby et al. (2015b). Chemical abundance analysis from Cohen & Huang (2009) reveals that the level of [C/Fe] in Dra strongly decreases around $[\text{Fe}/\text{H}] \sim -2.5$, such as the metallicity at which SNe Ia starts to kick in. Similarly, Sestito et al. (2023c) discovered that the contribution of SNe Ia in UMi starts at $[\text{Fe}/\text{H}] \sim -2.1$. In Sgr, the contribution of SNe Ia is absent in the VMP regime. However, Sestito et al. (2024b) suggest that the trend of [Co/Fe] at $[\text{Fe}/\text{H}] \gtrsim -2.0$ might be an indication of a possible contribution of SNe Ia in Sgr. This can also explain the lower [C/Fe] at $[\text{Fe}/\text{H}] \gtrsim -2.0$, compared to the more metal-poor bins. A more thorough investigation of this metallicity regime in Sgr will be explored by PIGS in a coming paper (Vitali et al., in prep.).

Sestito et al. (2024b) discussed the early chemical enrichment phase of Sgr from the detailed chemical abundances of 11 VMP stars. The chemical pattern of Sgr stars has been interpreted as the result of a mixture of Pop III and II stars

contributing (Sestito et al. 2024b). In particular, intermediate-mass high-energy and hypernovae are needed to explain the abundance patterns of the lighter elements up to the Fe-peak, while compact binary merger events and fast-rotating (up to $\sim 300 \text{ km s}^{-1}$) intermediate-mass to massive metal-poor stars ($\sim 25\text{--}120 M_{\odot}$) are needed to account for the level of the heavy elements. No evidence for contributions from pair-instability supernovae has been found in Sestito et al. (2024b). This mixture of various energetic SN events appears to be common in classical DGs and therefore explain the similarity in $[C/Fe]$ between these systems and their lower level compared to the MW (see the next section for a further discussion on this topic)

4.4. Various kinds of supernovae enrichment

The different amount of $[C/Fe]$ among the classical DGs and their lower level compared to the MW can be interpreted as the imprint of a different chemical evolution and a different efficiency in retaining the ejecta of SNe. For instance, the chemical evolution models from Vanni et al. (2023) suggested that DGs would have been polluted by a mixture of SNe II from Population III and II stars versus a more pristine population of SNe II in the building blocks of the MW halo (see also Skúladóttir et al. 2024b). The higher fraction of Pop II would have contributed to partially lower the average $[C/Fe]$ (Vanni et al. 2023).

In addition, the ISM of classical DGs is considered to be homogeneously mixed and, thus, able to retain the ejected yields from the most energetic events (Skúladóttir et al. 2024b), such as high-energy SNe II, hypernovae, and potential pair-instability SNe II. The retention of the ejected yields from the most energetic events would lower the average amount of $[C/Fe]$, given they would produce more Fe than C (e.g. Limongi & Chieffi 2018; Kobayashi et al. 2020; Koutsouridou et al. 2023; Vanni et al. 2023).

While there is a consensus that massive systems would contribute to the formation of the MW (e.g. Deason et al. 2016), an open question remains regarding whether the MW's building blocks resemble UFDs or DGs in terms of their ISM efficiency in retaining SNe yields or regarding their star formation history or their initial mass function. We interpret the higher average $[C/Fe]$ of the MW as an indication that the ISM efficiency of the MW's building blocks is similar to UFDs, hence unable to retain the most energetic events (e.g. Ji et al. 2016; Roederer et al. 2016; Hansen et al. 2017; Kobayashi et al. 2020; Applebaum et al. 2021; Waller et al. 2023; Sestito et al. 2024a). Therefore, the ISM of the building blocks of the MW, should be the fossil of the lower energetic events only (Koutsouridou et al. 2023; Vanni et al. 2023; Skúladóttir et al. 2024b). Additionally, if inhomogeneous chemical enrichment is in place, asymptotic giant branch stars (AGBs) can also be an extra source for the level of carbon, even at lower metallicities (Kobayashi et al. 2014; Vincenzo & Kobayashi 2018; Kobayashi et al. 2020).

Figure 5 also shows a difference in the average $[C/Fe]$ between the MW halo and the inner Galaxy, especially those stars confined within 3 kpc. Recently, Pagnini et al. (2023) suggested that a potential dearth of CEMP stars in the inner Galaxy could be due to the very high star formation rates at early times. The star formation would be so intense that stars massive enough to explode as pair-instability SNe would form, which would lower the average $[C/Fe]$ compared to the halo. However, no star carrying the imprint of pair-instability SNe has been found so far in the Galaxy (e.g. Lucey et al. 2022; Sestito et al. 2023b; Skúladóttir et al. 2024a).

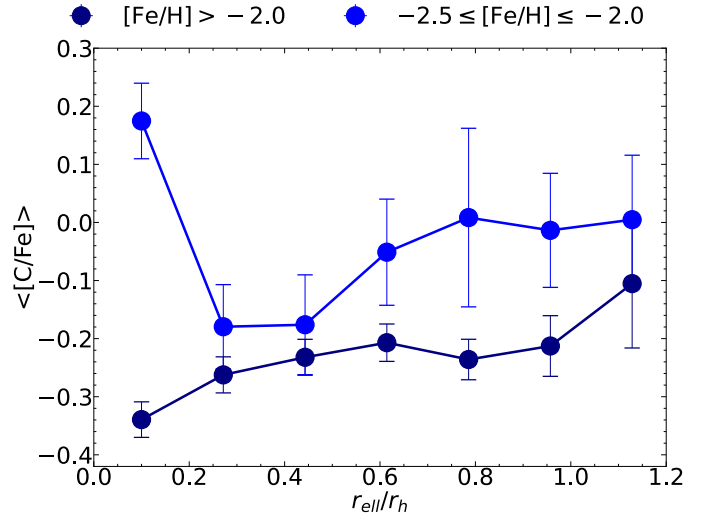


Fig. 6. Median $[C/Fe]$ as a function of the projected elliptical distance. Stars from the final selection of Sgr PIGS/AAT. The median is obtained removing the sample from CEMP stars and dividing it into distance bins and into two sub-groups, the more metal-poor (blue circles, $-2.5 \leq [Fe/H] \leq -2.0$) and the slightly more metal-rich (navy circles, $[Fe/H] > -2.0$). Stars have been selected to have $1.8 < \log g < 2.3$.

Furthermore, SNe Ia can concur to lower the average $[C/Fe]$ in a given system (Iwamoto et al. 1999). The contribution of SNe Ia might start at $[Fe/H] \gtrsim -2.5$ in some classical DGs (e.g. Cohen & Huang 2009; Venn et al. 2012; Kirby et al. 2015b; Sestito et al. 2023c), and likely between $-2.0 \lesssim [Fe/H] \lesssim -1.5$ for Sgr (Sestito et al. 2024b). This is not the case for the MW, where SNe Ia starts to kick in at higher metallicities, $[Fe/H] \sim -1.0$ (e.g. McWilliam 1997; Matteucci 2003; Venn et al. 2004). Therefore, the lower average $[C/Fe]$ at $[Fe/H] \gtrsim -2.5$ in DGs and at $[Fe/H] \gtrsim -2.0$ in Sgr can also be caused by the contribution of SNe Ia.

4.5. Radial gradient of $[C/Fe]$

Our sample is large enough and covers enough of Sgr to test whether there may be any radial gradients in $[C/Fe]$. To avoid potential systematic effects in $[C/Fe]$ between radial bins due to differences in stellar parameter coverage, we limit the sample to $1.8 < \log g < 2.3$ for this analysis. We find that the general picture of our results does not change compared to using a more generous cut or the full sample, but the behaviour is cleaner for the limited sample.

The median $[C/Fe]$ as a function of the projected elliptical distance is shown in Fig. 6. The Sgr PIGS/AAT sample is divided into two sub-groups, the low-metallicity (blue circles, $-2.5 \leq [Fe/H] \leq -2.0$) and a slightly more metal-rich group (navy circles, $-2.0 < [Fe/H] \leq -1.5$), and removing CEMP stars from the calculations. There is a net positive $[C/Fe]$ gradient for the slightly more metal-rich sub-group, with a difference of $\sim +0.25$ dex between the very inner region and the outskirts of Sgr. This leads to a positive gradient in $[C/Fe]$ of about $\nabla[C/Fe] \sim 0.23 \text{ dex } r_h^{-1}$ or $\sim 8.8 \times 10^{-2} \text{ dex kpc}^{-1}$ or $\sim 6.8 \times 10^{-4} \text{ dex arcmin}^{-1}$.

Regarding the low-metallicity sub-group, a mild positive gradient is visible if the innermost bin is not considered. In this case, the difference in $[C/Fe]$ would be ~ 0.2 dex between the inner to the outer Sgr's regions. To be taken into account, uncertainties

on the average $[C/Fe]$ are larger for the low-metallicity sub-group than the more metal-rich one.

We consider whether the more pronounced gradient at higher metallicities are connected to a different chemical enrichment between the two populations. A couple of concurrent mechanisms might explain these gradients: outside-in star formation and the contribution of SNe Ia.

The former, as discussed in Sect. 3, implies that the oldest and most metal-poor stars should form everywhere in the system and would carry a similar imprint of nucleosynthetic events, if homogeneous mixing is also applied to the system. In the case that the ISM is not completely homogeneously mixed between the inner regions and the outskirts, these two regions might carry different level of $[C/Fe]$. It is likely that the outskirts would be less efficient in retaining the more energetic events as the inner regions, resulting in a higher average $[C/Fe]$.

The stellar feedback from the first supernovae would expel the gas outside the system, which then later would be re-accreted onto the inner regions, where slightly more metal-rich stars would form. These relatively metal-richer inner stars might carry the imprint of SNe Ia as well. As discussed in Sect. 4.4, SNe Ia can lower the average $[C/Fe]$ (Iwamoto et al. 1999), and the higher contribution of these events in the inner regions would explain the positive gradient in $[C/Fe]$. This result would be an indication, in addition to the trend of $[Co/Fe]$ in Sestito et al. (2024b), that SNe Ia might have started to kick in in Sgr at metallicities between $-2.0 < [Fe/H] < -1.5$, well below what was previously inferred ($[Fe/H] \sim -1.27$, e.g. de Boer et al. 2014).

5. CEMP stars

As discussed in the Introduction, CEMP stars are of interest because they probe the properties of the First Stars and early chemical evolution (CEMP-no) and of binary populations (CEMP-s). Next, we investigate the properties of CEMP stars in Sgr with the PIGS/AAT Sgr data set, which is much larger than previous literature samples with $[C/Fe]$ in Sgr.

To our sample of carbon measurements in Sgr, we added those of Chiti & Frebel (2019) and Chiti et al. (2020), who observed metal-poor Sgr stars with the Magellan Echelle (MagE) Spectrograph, measuring $[C/Fe]$ for 4 and 18 targets, respectively. These stars have metallicities in the range $-3.1 \lesssim [Fe/H] \lesssim -1.5$, similarly to the PIGS/AAT range. None of these stars are CEMP according to the standard definition ($[C/Fe] > +0.7$). Other Sgr members with measured $[C/Fe]$ that are not included are the targets analysed in Hansen et al. (2018a) and from APOGEE DR17. Hansen et al. (2018a) measured $[C/Fe]$ in 12 stars with metallicity $-2.95 \lesssim [Fe/H] \lesssim -1.40$. These targets were observed with UVES high-resolution spectrograph at VLT. However, as shown in Sestito et al. (2024b), the $[C/Fe]$ ratios from Hansen et al. (2018a) are systematically lower than the ones from Chiti & Frebel (2019), Chiti et al. (2020), and this work (see Fig. 5 in Sestito et al. 2024b). APOGEE stars are not included, since the C-measurements are in non-local thermodynamic equilibrium (non-LTE) and in the infra-red, which have offsets compared to LTE measurements in the optical (Jönsson et al. 2020).

5.1. New CEMP stars in Sgr

The distribution of $[Fe/H]$ versus $A(C)$ for Sgr stars is shown in Fig. 7 (blue circles). According to the classical definition of CEMP stars ($[C/Fe] > +0.7$), only three or four stars in the PIGS/AAT Sgr sample are classified as CEMP. One of them

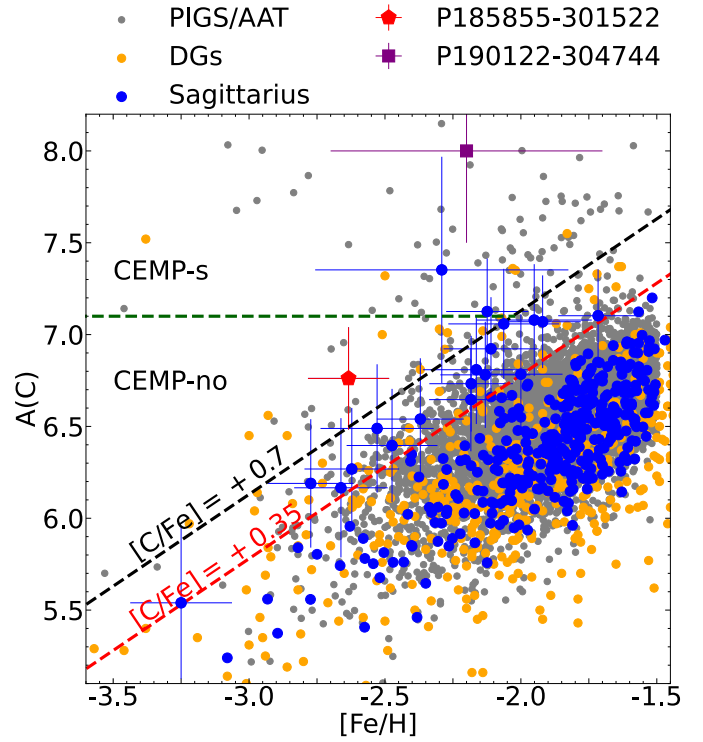


Fig. 7. Abundance of C, $A(C)$, as a function of $[Fe/H]$. The Sagittarius sample (blue circles) includes stars from the final selection made in Sect. 2.3, from Chiti & Frebel (2019), and from Chiti et al. (2020). The DGs compilation (orange circles) is from Lucchesi et al. (2024). Inner Galaxy stars (grey circles) are selected from Ardern-Arentsen et al. (2024) to have good quality of the AAT spectra and good FERRE measurements as in our sample. Star P185855–301522 (red pentagon) is analysed in Sestito et al. (2024b) and confirmed to be CEMP-s from high-resolution spectroscopy. Star P190122-304744 (purple square) is one of the two cool CEMP candidates discussed in Sect. 5.2. Horizontal green dashed line tentatively separates CEMP-s from CEMP-no as in Yoon et al. (2016). Stars on the left of the dashed black line have $[C/Fe] > +0.7$ as defined in Aoki et al. (2007). The dashed red line denotes the tentative new limit for CEMP in Sgr ($[C/Fe] = +0.35$). Sgr stars with $[C/Fe] > +0.35$ are displayed with their errorbars to highlight that they are significantly distant from the bulk of the system's distribution.

(red pentagon) has previously been studied in Sestito et al. (2024b), and was confirmed to be a CEMP-s star based on the over-abundance of s-process elements ($[Ba/Fe] \sim +1.2$). For the other two CEMP candidates, Ba measurements are not available. We compare the distribution of metallicities and carbon abundances with those for the inner Galaxy (grey circles) and DGs (Lucchesi et al. 2024, orange circles). We note that the DG sample only includes carbon-normal and spectroscopically confirmed CEMP-no stars.

Without measurements of Ba or Sr, it is not possible to classify CEMP stars with certainty, although a rough classification can be made based on $[Fe/H]$ and $A(C)$ alone (e.g. Yoon et al. 2016). CEMP-s stars typically have higher $A(C)$ than CEMP-no stars and are more common at higher metallicities, and a tentative separation between the two groups has been placed at $A(C) = 7.1$ (Yoon et al. 2016) and $[Fe/H] \gtrsim -3.3$. It is not entirely clean – there is some known contamination when using such a simple division without detailed chemistry, for example the Sestito et al. (2024b) CEMP-s star lies in the CEMP-no region based on $[Fe/H]$ and $A(C)$ alone, and some DG CEMP-no stars

lie in the CEMP-s region. Similarly, a contamination of CEMP-no in the CEMP-s region is also found for MW halo stars (e.g. Norris & Yong 2019). However, without better data, we may propose that the two new Sgr CEMP stars are likely of the CEMP-s kind given their metallicity and high carbon abundances.

5.2. Two cool candidate CEMP stars

We noticed that there are two stars in the AAT/Sgr sample (not passing our FERRE quality cuts, based on χ^2) that by eye appear to be very carbon-rich from their spectrum. These stars, Pristine_185524.38-291422.5 (Gaia DR3 source_id = 6761678859361894912) and Pristine_190122.55-304744.3 (6760545743905626496) are highlighted with pink circles in the Pristine colour-colour diagram in the top left and right panels of Fig. 1. It is curious that one of them is located above the primary Sgr sequence in the Pristine colour-colour diagram. They are also shown on the CMD with large red symbols in the top panel of Fig. 8. The same star that is an outlier in the colour-colour diagram is located beyond the metal-rich side of the RGB, which is also curious. If the star is truly a Sgr star (and there is no reason to suspect it is not given its radial velocity and proper motions), it cannot be an intrinsic carbon star, because it is not evolved enough.

Both stars have FERRE $T_{\text{eff}} \sim 4500$ K, which is at the cool boundary of the FERRE grid; thus, they might actually be even cooler. An inspection of the spectroscopic fit shows that the FERRE fit is bad in both the blue and the CaT regions: there is a strong discrepancy between the carbon features in the star and those in the FERRE grid, although it is clear that the star is very carbon-rich. This is potentially due to the assumptions on nitrogen in the FERRE grid (see below).

To further constrain the stellar parameters for these stars, we employ a different grid of synthetic spectra originally created for use in the Segue Stellar Parameter Pipeline (SSPP, Lee et al. 2008a,b, grid from Y.S. Lee, private communication). An important difference between the FERRE and SSPP grids is that the former assumes $[\text{N}/\text{Fe}] = 0$, while the latter assumes $[\text{C}/\text{N}] = 0$ – this is potentially particularly important for fitting the CN features in the CaT. We use a cool subset of the grid with the following stellar parameters: $T_{\text{eff}} = [4000, 4250, 4500, 4750]$ K, $\log g = 1.0$ (we checked that varying $\log g$ does not make a difference), $[\text{Fe}/\text{H}]$ from -3.0 to -1.0 in steps of 0.25 dex and $[\text{C}/\text{Fe}]$ from 0.0 to +3.0 in steps of 0.25 dex. After normalising both the observed and synthetic spectra with a running median of 200 pixels (50 \AA), we search for the best matching spectrum by minimising the residuals. We do this separately for the CaT and the blue and combine the χ^2 values afterwards, giving more weight to the CaT because of its high resolution and because it is less sensitive to the shape of the molecular bands.

For both of the stars there is no clear best-fit stellar parameter combination, because there are strong degeneracies between T_{eff} , $[\text{Fe}/\text{H}]$ and $[\text{C}/\text{Fe}]$. For Pristine_185524.38-291422.5, the outlier in photometry, the main constraint is placed on the absolute carbon abundance: for the 5% best fits, $A(\text{C}) = 8.7 \pm 0.4$ (mean and standard deviation). The mean metallicity is -1.5 ± 0.4 and the temperature is not well-constrained within the limit of our small grid. The other star, Pristine_190122.55-304744.3, is more metal-poor and slightly less carbon-rich – the mean $A(\text{C}) = 8.0 \pm 0.5$ and $[\text{Fe}/\text{H}] = -2.2 \pm 0.5$ for the 5% best fits, and the temperature is again not well-constrained. For each of these stars, we present one of the best matching synthetic spectra in Fig. 8, with the observed spectrum in black and the synthetic one in red. We applied a by-eye linear normalisation to the blue arm synthetic

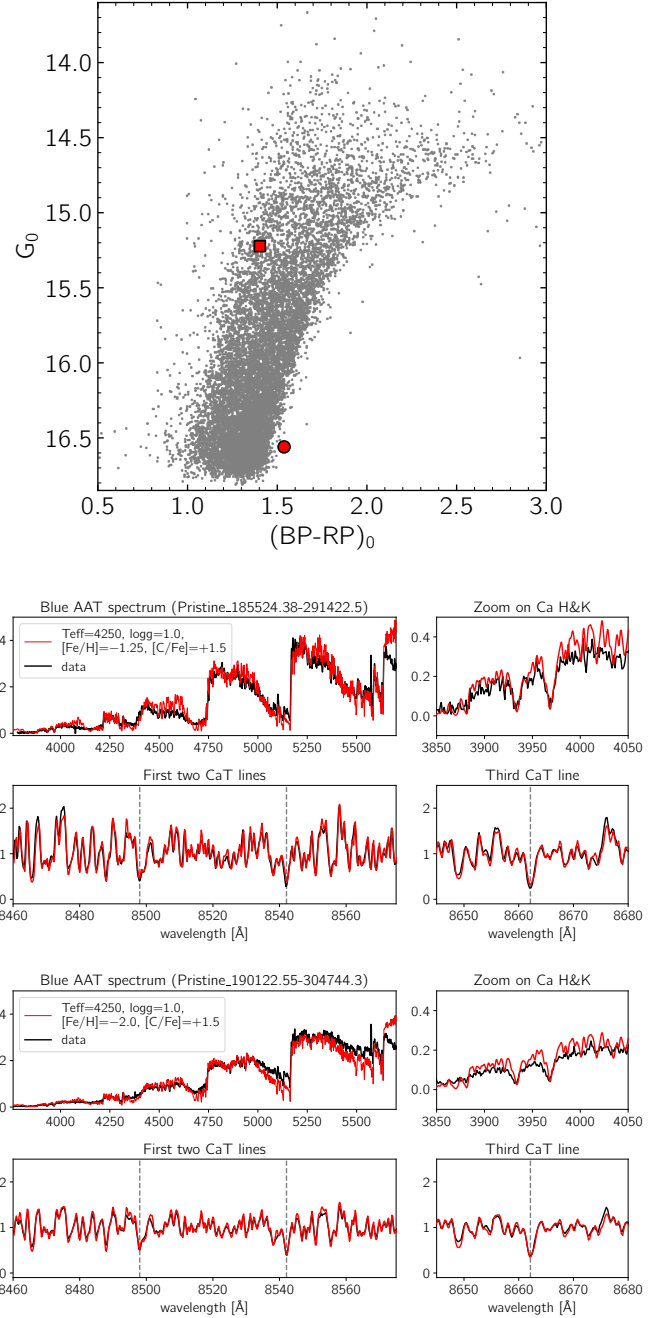


Fig. 8. Colour–magnitude diagram of stars in Sagittarius (top, with the same samples as grey dots in Fig. 1), with the CEMP candidates Pristine_185524.38-291422.5 (circle) and Pristine_190122.55-304744.3 (square) highlighted with large red symbols. Middle: one of the best matching spectra from the SSPP synthetic grid for Pristine_185524.38-291422.5 on top of its AAT spectrum. Bottom: Same but for Pristine_190122.55-304744.3.

spectrum to roughly match the shape of the observed spectrum rather than showing the normalised version, so the match is not perfect.

We conclude that these stars are likely CH- or CEMP-s stars. The location of the more metal-rich star in the Pristine colour-colour diagram and the CMD is likely strongly affected by the very large carbon bands, causing the star to look fainter and redder compared to where a ‘normal’ metal-poor star would be. This effect appears to be less strong for the more metal-poor

star, although it is on the border of having been included in our selection according to Fig. 1. Such extreme stars have likely been missed in other selections of metal-poor stars as well, in DGs and the Milky Way, possibly leading to an underestimate of the number of binary mass-transfer type stars at intermediate metal-poor metallicities.

5.3. Fraction of CEMP stars

In the Galactic halo, the cumulative fraction of CEMP stars for $[\text{Fe}/\text{H}] < -2.0$ has been found to be of the order of 20–30%, rising to 30–40% for $[\text{Fe}/\text{H}] < -3.0$ (Lee et al. 2013; Placco et al. 2014; Arentsen et al. 2021). There are various caveats complicating the exact determination of the overall CEMP and separate CEMP-no and CEMP-s fractions in the Galactic halo (Arentsen et al. 2021), but the consensus is that there is a significant fraction of these stars at low metallicity. As shown in Fig. 7, only three out of 356 PIGS/AAT Sgr stars is classified as CEMP and none from Chiti & Frebel (2019) and Chiti et al. (2020), giving a total percentage of $\sim 3\%$ for $[\text{Fe}/\text{H}] < -2.0$ and $\sim 5\%$ for $[\text{Fe}/\text{H}] < -2.5$ – much lower than that claimed in Galactic halo samples. This could partially be the result of our photometric metal-poor candidate selection being biased against carbon-rich stars, especially those at slightly higher metallicity ($[\text{Fe}/\text{H}] > -2.5$) and/or higher carbon abundance ($[\text{C}/\text{Fe}] > +1.5$) – the realm of the CEMP-s stars.

The CEMP fraction in Sgr is also low for $[\text{Fe}/\text{H}] < -2.5$, and we find that none of the 8 Sgr stars with $[\text{Fe}/\text{H}] < -2.7$ are CEMP. This is interesting given that in our test of the selection function in Sect. 2.2, we found that CEMP-no stars in this metallicity range should typically not have been excluded from our selection. This finding is consistent with previous observations suggesting that classical DGs are poor in CEMP-no stars in comparison to the MW and UFDs (e.g. Starkenburg et al. 2013; Jablonka et al. 2015; Kirby et al. 2015b; Simon et al. 2015; Hansen et al. 2018b; Lucchesi et al. 2024; Skúladóttir et al. 2015, 2021, 2024b; Chiti et al. 2024).

5.4. Redefining CEMP stars in DGs

Given that the average carbon abundance is ~ 0.3 dex lower in Sgr compared to the Milky Way (Fig. 5), is it fair to use the same definition of carbon-enhancement as in the Milky Way? This seems to be a generic question for classical DGs, as most of them have lower average $[\text{C}/\text{Fe}]$ than the Milky Way, as discussed in the previous section, and they would therefore need a larger carbon “boost” to be classified as CEMP. The LMC also has lower carbon abundances compared to the MW halo (although similar to the inner Galaxy), with a dearth of CEMP stars (Jönsson et al. 2020; Chiti et al. 2024; Oh et al. 2024). The first definition of CEMP stars was $[\text{C}/\text{Fe}] > +1.0$ (Beers & Christlieb 2005), which was refined empirically by Aoki et al. (2007) to $[\text{C}/\text{Fe}] > +0.7$ based on a sample of observations of MW stars, using the gap between carbon-normal stars and outliers with high carbon abundances. This definition is therefore a relative one, specifically for the Milky Way ‘field’ population, raising the question whether it ought to be redefined for dwarf galaxies.

Inspecting Fig. 7, there are a significant number of Sgr stars that appear to be outliers in A(C) from the main Sgr trend, although they do not make it to above the classical CEMP definition of $[\text{C}/\text{Fe}] > +0.7$. For $[\text{Fe}/\text{H}] \lesssim -2.5$ in the PIGS/AAT inner Galaxy sample, the average $[\text{C}/\text{Fe}] \approx +0.3$ with a dispersion of 0.2 dex (conservative estimate) – meaning that the $[\text{C}/\text{Fe}] = +0.7$ CEMP definition selects stars that are $\sim 2\sigma$ outliers, roughly

0.4 dex higher than the mean trend. The average $[\text{C}/\text{Fe}]$ in Sgr in the lowest metallicity bins ($[\text{Fe}/\text{H}] \lesssim -2.5$) is ~ -0.05 ; therefore, by adopting a similar conservative dispersion, stars with $[\text{C}/\text{Fe}] > -0.05 + 0.4 > +0.35$ could be considered outliers in Sgr (and, thus, CEMPs). This working definition of CEMP stars in Sgr is shown in Fig. 7 with a dashed red line. Using this new definition, ~ 20 Sgr members would be classified as CEMP stars (vs 3–4 from the classical definition). This would lead to a carbon-enhanced percentage of $\sim 15\%$ for $[\text{Fe}/\text{H}] < -2.0$, which is much less in tension with the results in the MW (20–30%, Lee et al. 2013; Placco et al. 2014; Arentsen et al. 2021). The percentage would be $\sim 12\%$ for $-2.5 < [\text{Fe}/\text{H}] < -2.0$ and $\sim 30\%$ for $[\text{Fe}/\text{H}] < -2.5$ (or $\sim 35\%$ if only Sgr/AAT data are considered), compatible with the frequency of CEMP stars in the MW.

Similarly, for Dra, UMi, and Scl (selecting stars between $-2.4 < [\text{Fe}/\text{H}] < -1.9$), the new $[\text{C}/\text{Fe}]$ threshold for a member star to be a CEMP would be $\sim +0.3, +0.3, +0.1$, respectively. This new limit would suggest that the percentage of CEMP in Dra, UMi, and Scl would be $\sim 16\%, 27\%, 19\%$, respectively. However, the latter values refer only to the CEMP-no population, given that the compilation from Lucchesi et al. (2024) does not contain CEMP-s stars.

We want to highlight that our new definition of CEMP is strictly empirical and based on the position of outliers in the $[\text{C}/\text{Fe}]$ or A(C) distribution – they could be enhanced in carbon for a number of reasons. A more physically driven definition should take into account the IMF and the energy ranges of the SNe II exploded in a given system, the contribution of SN Ia and AGBs, the binary fraction, and the efficiency of the system’s ISM in recycling the ejected yields. Additionally, investigations of the chemical properties of CEMP candidates based on our relative CEMP definition will be necessary to test whether they show differences in their abundance patterns compared to stars in the bulk of the carbon-metallicity distribution, and whether they are truly a different population of stars.

6. Summary

The chemo-dynamical properties of the low-metallicity regime of the Sagittarius dwarf galaxy are explored using the low- and medium-resolution AAT spectra observed by the Pristine Inner Galaxy Survey (PIGS). The PIGS dataset contains measurements of RVs, stellar parameters, $[\text{Fe}/\text{H}]$, and $[\text{C}/\text{Fe}]$ for stars towards the inner Galaxy and Sgr. We summarise our main conclusions below:

1. We provide a clean list of low-metallicity ($[\text{Fe}/\text{H}] \leq -1.5$) members stars selected according to their RV from AAT and proper motion and on-sky position from Gaia, as in Vitali et al. (2022), and updated to DR3 (Fig. 2). A table updated based on Gaia DR3 has been made available online;
2. The metal-poor ($[\text{Fe}/\text{H}] \leq -1.5$) population (PIGS/AAT) of Sgr has a larger velocity dispersion and systemic RV than the metal-rich ($[\text{Fe}/\text{H}] \geq -0.6$, APOGEE) as shown in Figs. 3 and 4. Additionally, the velocity dispersion and the systemic RV increase in the outer regions for both populations. This effect might be caused by the contribution of various mechanisms, such as the complex structure in Sgr (MR/disc + MP/halo), the outside-in star formation, and the extreme Galactic tidal perturbations acting in the system;
3. The average $[\text{C}/\text{Fe}]$ of Sgr is similar to the range displayed by the other classical DGs (Fig. 5). However, the level of $[\text{C}/\text{Fe}]$ is higher in Sgr than in Car and Scl. This can be explained by differences in the IMF and in the energy distribution of the

SNe II among these systems, with a predominance of more energetic events in Car and Scl;

4. The average $[C/Fe]$ of Sgr, and of the other classical DGs, is lower than in the MW at fixed $[Fe/H]$ when compared to either inner Galactic or halo-like stars (Fig. 5). The ISM of classical DGs might have been able to retain the ejecta of energetic events, such as hypernovae. However, this would not have been the case for the building blocks of the Galaxy, where stochasticity might have played an important role. In this scenario, classical DGs should display the imprint of Population III and II high-energy SNe II, which would act to lower the average $[C/Fe]$. Instead, less energetic events, as well as faint- and core-collapse SNe II from a more pristine population, should be imprinted in the stars of the MW building blocks; hence, the higher $[C/Fe]$. On the other hand, some studies (e.g. Deason et al. 2016) suggest that the majority of the MW building blocks should be similar in size to present DGs. However, their chemical evolution still remain an open question. Our results indicate a different supernovae imprint between Sgr (and classical DGs) versus the MW building blocks;
5. SNe Ia can also lower the average $[C/Fe]$. This kind of event would be already present at $[Fe/H] \sim -2.0$ in classical DGs and absent in the MW stars at the same metallicities. Indications of the SNe Ia contributions in Sgr starting at $-2.0 < [Fe/H] < -1.5$ are the lower median $[C/Fe]$ at these metallicities vs the higher $[C/Fe]$ at lower metallicities (see Fig. 5) and also the lower $[C/Fe]$ in the inner regions (see Fig. 6), inhabited by a slightly more metal-rich population. The presence of SNe Ia at the aforementioned metallicities would also be confirmed by the trend of $[Co/Fe]$ found by Sestito et al. (2024b);
6. We find a positive $[C/Fe]$ gradient of $\nabla[C/Fe] \sim 0.23 \text{ dex } r_h^{-1}$ or $\sim 8.8 \times 10^{-2} \text{ dex kpc}^{-1}$ or $\sim 6.8 \times 10^{-4} \text{ dex arcmin}^{-1}$ for stars with $-2.0 < [Fe/H] < -1.5$ (Fig. 6), which we interpret as the effect of contributions by SNe Ia;
7. We identified four new CEMP stars in Sgr. Figure 7 suggests that the empirical distinction between CEMP-s and CEMP-no solely based on $A(C)$ does not work well for Sgr and the classical DGs. We therefore cannot reach definitive conclusions on the nature of the new CEMP stars, however, we propose that they are likely to be of the CEMP-s type, given their $[Fe/H]$ and high $A(C)$;
8. The AAT spectra of two carbon-rich candidates, Pristine_185524.38-291422.5 and Pristine_190122.55-304744.3, were re-analysed with the SSPP grid of synthetic spectra (Fig. 8) because they had high χ^2 in the FERRE fit and were at the edge of the FERRE grid. They were shown to exhibit $[Fe/H] \sim -1.5$ and -2.2 with very high carbon abundances $A(C) \sim 8.8$ and 8.0 , respectively, making them CH- or CEMP-s candidates. The C-bands of the former star strongly affect its colour, magnitude and its position in the Pristine colour-colour diagram (Figs. 1 and 8). Similar stars could have been missed in other metal-poor (DG) selections as well;
9. The photometric selection effects in the various PIGS fields that include Sgr targets are discussed, showing there is a bias against CEMP stars in the sample (Fig. 1); specifically, those of the CEMP-s (binary interaction) type. CEMP-no stars (connected to early chemical evolution). However, are less likely to have been excluded from the selection and their frequency in our sample should be largely unbiased;
10. Following the classical definition of CEMP stars ($[C/Fe] > +0.7$), the fraction of CEMP stars in our sample is very low:

$\sim 3\%$ for $[Fe/H] < -2.0$ and $\sim 6\%$ for $[Fe/H] < -2.5$. However, the low mean abundance of $[C/Fe]$ in Sgr (and other classical DGs), along with the clear presence of outliers of the distribution at ‘intermediate’ carbon abundances, leads us to propose a new definition for CEMP stars. Rather than a fixed threshold, the limit should depend on the average $[C/Fe]$ of a given system. For Sgr, stars with $[C/Fe] \gtrsim +0.35$ can be considered CEMP in this case, as they are outliers from the bulk of the system’s distribution (see Fig. 7). The new frequency of CEMP in Sgr according to this definition would be $\sim 12\%$ for $-2.5 < [Fe/H] < -2.0$ and $\sim 30\text{--}35\%$ for $[Fe/H] < -2.5$, which is in much better agreement with the frequencies in the MW.

This work, which stands as a complement to the high-resolution investigation by Sestito et al. (2024b), provides a novel glimpse into the early chemical evolution of Sgr by exploring its carbon levels. These works will be beneficial for upcoming spectroscopic surveys, for example, 4DWARFS (Skúladóttir et al. 2023), which is poised to observe a larger number of stars in the Sgr core and in its streams.

Data availability

The updated list of Sagittarius members is available at the CDS via anonymous ftp to cdsarc.cds.unistra.fr (130.79.128.5) or via <https://cdsarc.cds.unistra.fr/viz-bin/cat/J/A+A/690/A333>

Acknowledgements. We acknowledge and respect the ləkʷəŋən peoples on whose traditional territory the University of Victoria stands and the Songhees, Esquimalt and WSÁNEĆ peoples whose historical relationships with the land continue to this day. We thank the Australian Astronomical Observatory, which have made the PIGS spectroscopic follow-up observations used in this work possible. We acknowledge the traditional owners of the land on which the AAT stands, the Gamilaraay people, and pay our respects to elders past and present. We want to thank the anonymous referee for their helpful and insightful comments. We thank Vini Placco for calculating the carbon evolutionary corrections. We thank Young Sun Lee for providing the SSPP synthetic spectra. FS and KAV thank the National Sciences and Engineering Research Council of Canada for funding through the Discovery Grants and CREATE programs. AAA acknowledges support from the Herchel Smith Fellowship at the University of Cambridge and a Fitzwilliam College research fellowship supported by the Isaac Newton Trust. SV thanks ANID (Beca Doctorado Nacional, folio 21220489) and Universidad Diego Portales for the financial support provided. SV acknowledges the Millennium Nucleus ERIS (ERIS NCN2021017) and FONDECYT (Regular number 1231057) for the funding. NFM gratefully acknowledges support from the French National Research Agency (ANR) funded project ‘Pristine’ (ANR-18-CE31-0017) along with funding from the European Research Council (ERC) under the European Union’s Horizon 2020 research and innovation programme (grant agreement No. 834148). ES acknowledges funding through VIDI grant ‘Pushing Galactic Archaeology to its limits’ (with project number VI.Vidi.193.093) which is funded by the Dutch Research Council (NWO). This research has been partially funded from a Spinoza award by NWO (SPI 78-411). The spectroscopic follow-up used in this work was based on selection from observations obtained with MegaPrime/MegaCam, a joint project of CFHT and CEA/DAPNIA, at the Canada–France–Hawaii Telescope (CFHT) which is operated by the National Research Council (NRC) of Canada, the Institut National des Science de l’Univers of the Centre National de la Recherche Scientifique (CNRS) of France, and the University of Hawaii. This work has made use of data from the European Space Agency (ESA) mission *Gaia* (<https://www.cosmos.esa.int/gaia>), processed by the *Gaia* Data Processing and Analysis Consortium (DPAC, <https://www.cosmos.esa.int/web/gaia/dpac/consortium>). Funding for the DPAC has been provided by national institutions, in particular the institutions participating in the *Gaia* Multilateral Agreement. This research has made use of the SIMBAD database, operated at CDS, Strasbourg, France (Wenger et al. 2000). This work made extensive use of TOPCAT (Taylor 2005). *Author contribution statement.* FS led the analysis and the various discussions in this work, contributed to write most of this draft, and created most of the Figures. AAA led the PIGS/AAT target selection and observations, coded the PIGS/AAT spectroscopic analysis with David Aguado (not a co-author

here), analysed the cool candidate CEMP stars discussed in Section 5.2, created the respective section with figures, and was closely involved in shaping the manuscript and contributed to the scientific discussion. SV contributed to the discussion and revision of the paper. MM identified one of the cool candidate CEMP stars using photometry and contributed to the discussion. RL provided the [C/Fe] dataset of the various dwarf galaxies. KAV, NFM, JFN, and ES provided insightful scientific and editorial comments on the manuscript.

References

- Abate, C., Pols, O. R., Izzard, R. G., Mohamed, S. S., & de Mink, S. E. 2013, *A&A*, 552, A26
- Abdurro'uf, Accetta, K., Aerts, C., et al. 2022, *ApJS*, 259, 35
- Aguado, D. S., Youakim, K., González Hernández, J. I., et al. 2019, *MNRAS*, 490, 2241
- Allende Prieto, C., Beers, T. C., Wilhelm, R., et al. 2006, *ApJ*, 636, 804
- An, Z., Walker, M. G., & Pace, A. B. 2024, arXiv e-prints [arXiv:2404.16184]
- Aoki, W., Beers, T. C., Christlieb, N., et al. 2007, *ApJ*, 655, 492
- Applebaum, E., Brooks, A. M., Christensen, C. R., et al. 2021, *ApJ*, 906, 96
- Ardern-Arentsen, A., Monari, G., Queiroz, A. B. A., et al. 2024, *MNRAS*, 530, 3391
- Arentsen, A., Starkenburg, E., Martin, N. F., et al. 2020a, *MNRAS*, 496, 4964
- Arentsen, A., Starkenburg, E., Martin, N. F., et al. 2020b, *MNRAS*, 491, L11
- Arentsen, A., Starkenburg, E., Aguado, D. S., et al. 2021, *MNRAS*, 505, 1239
- Arentsen, A., Placco, V. M., Lee, Y. S., et al. 2022, *MNRAS*, 515, 4082
- Arroyo-Polonio, J. M., Battaglia, G., Thomas, G. F., et al. 2023, *A&A*, 677, A95
- Battaglia, G., Tolstoy, E., Helmi, A., et al. 2006, *A&A*, 459, 423
- Battaglia, G., Helmi, A., Tolstoy, E., et al. 2008, *ApJ*, 681, L13
- Battaglia, G., Taibi, S., Thomas, G. F., & Fritz, T. K. 2022, *A&A*, 657, A54
- Beers, T. C., & Christlieb, N. 2005, *ARA&A*, 43, 531
- Beers, T. C., Rossi, S., Norris, J. E., Ryan, S. G., & Sheffer, T. 1999, *AJ*, 117, 981
- Bellazzini, M., Ferraro, F. R., & Buonanno, R. 1999, *MNRAS*, 307, 619
- Bellazzini, M., Ibata, R. A., Chapman, S. C., et al. 2008, *AJ*, 136, 1147
- Belokurov, V., & Kravtsov, A. 2022, *MNRAS*, 514, 689
- Belokurov, V., & Kravtsov, A. 2023, *MNRAS*, 525, 4456
- Belokurov, V., Koposov, S. E., Evans, N. W., et al. 2014, *MNRAS*, 437, 116
- Benítez-Llambay, A., Navarro, J. F., Abadi, M. G., et al. 2016, *MNRAS*, 456, 1185
- Bonifacio, P., Hill, V., Molaro, P., et al. 2000, *A&A*, 359, 663
- Caffau, E., Bonifacio, P., Sbordone, L., et al. 2020, *MNRAS*, 493, 4677
- Carlberg, R. G., & Grillmair, C. J. 2022, *ApJ*, 935, 14
- Chiti, A., & Frebel, A. 2019, *ApJ*, 875, 112
- Chiti, A., Hansen, K. Y., & Frebel, A. 2020, *ApJ*, 901, 164
- Chiti, A., Frebel, A., Simon, J. D., et al. 2021, *Nat. Astron.*, 5, 392
- Chiti, A., Mardini, M., Limberg, G., et al. 2024, *Nat. Astron.*, 8, 637
- Choi, J., Dotter, A., Conroy, C., et al. 2016, *ApJ*, 823, 102
- Chou, M.-Y., Majewski, S. R., Cunha, K., et al. 2007, *ApJ*, 670, 346
- Cohen, J. G., & Huang, W. 2009, *ApJ*, 701, 1053
- Cunningham, E. C., Hunt, J. A. S., Price-Whelan, A. M., et al. 2024, *ApJ*, 963, 95
- Da Costa, G. S., Bessell, M. S., Mackey, A. D., et al. 2019, *MNRAS*, 489, 5900
- de Boer, T. J. L., Belokurov, V., Beers, T. C., & Lee, Y. S. 2014, *MNRAS*, 443, 658
- Deason, A. J., Mao, Y.-Y., & Wechsler, R. H. 2016, *ApJ*, 821, 5
- del Pino, A., Fardal, M. A., van der Marel, R. P., et al. 2021, *ApJ*, 908, 244
- Dotter, A. 2016, *ApJS*, 222, 8
- Fernández-Alvar, E., Kordopatis, G., Hill, V., et al. 2021, *MNRAS*, 508, 1509
- Filion, C., & Wyse, R. F. G. 2021, *ApJ*, 923, 218
- Frebel, A., Johnson, J. L., & Bromm, V. 2007, *MNRAS*, 380, L40
- Gaia Collaboration (Prusti, T., et al.) 2016, *A&A*, 595, A1
- Gaia Collaboration (Brown, A. G. A., et al.) 2018, *A&A*, 616, A1
- Gaia Collaboration (Brown, A. G. A., et al.) 2021, *A&A*, 649, A1
- Gaia Collaboration (Vallenari, A., et al.) 2023, *A&A*, 674, A1
- Gibbons, S. L. J., Belokurov, V., & Evans, N. W. 2017, *MNRAS*, 464, 794
- Goswami, A., Aoki, W., Beers, T. C., et al. 2006, *MNRAS*, 372, 343
- Gray, E. I., Read, J. I., Taylor, E., et al. 2024, *MNRAS*, submitted [arXiv:2405.19286]
- Hansen, T. T., Simon, J. D., Marshall, J. L., et al. 2017, *ApJ*, 838, 44
- Hansen, C. J., El-Soury, M., Monaco, L., et al. 2018a, *ApJ*, 855, 83
- Hansen, T. T., Holmbeck, E. M., Beers, T. C., et al. 2018b, *ApJ*, 858, 92
- Hasselquist, S., Shetrone, M., Smith, V., et al. 2017, *ApJ*, 845, 162
- Hasselquist, S., Hayes, C. R., Lian, J., et al. 2021, *ApJ*, 923, 172
- Hayes, C. R., Majewski, S. R., Hasselquist, S., et al. 2020, *ApJ*, 889, 63
- Hayes, C. R., Venn, K. A., Waller, F., et al. 2023, *ApJ*, 955, 17
- Helmi, A. 2020, *ARA&A*, 58, 205
- Herlan, R., Mastrobuono-Battisti, A., & Neumayer, N. 2023, *MNRAS*, 523, 2721
- Hidalgo, S. L., Monelli, M., Aparicio, A., et al. 2013, *ApJ*, 778, 103
- Howes, L. M., Asplund, M., Casey, A. R., et al. 2014, *MNRAS*, 445, 4241
- Howes, L. M., Casey, A. R., Asplund, M., et al. 2015, *Nature*, 527, 484
- Howes, L. M., Asplund, M., Keller, S. C., et al. 2016, *MNRAS*, 460, 884
- Ibata, R. A., Gilmore, G., & Irwin, M. J. 1994, *Nature*, 370, 194
- Iwamoto, K., Brachwitz, F., Nomoto, K., et al. 1999, *ApJS*, 125, 439
- Iwamoto, N., Umeda, H., Tominaga, N., Nomoto, K., & Maeda, K. 2005, *Science*, 309, 451
- Jablonka, P., North, P., Mashonkina, L., et al. 2015, *A&A*, 583, A67
- Jensen, J., Hayes, C. R., Sestito, F., et al. 2024, *MNRAS*, 527, 4209
- Ji, A. P., Frebel, A., Chiti, A., & Simon, J. D. 2016, *Nature*, 531, 610
- Johnson, B. D., Conroy, C., Naidu, R. P., et al. 2020, *ApJ*, 900, 103
- Jönsson, H., Holtzman, J. A., Allende Prieto, C., et al. 2020, *AJ*, 160, 120
- Kacharov, N., Alfaro-Cuello, M., Neumayer, N., et al. 2022, *ApJ*, 939, 118
- Kazantzidis, S., Łokas, E. L., Callegari, S., Mayer, L., & Moustakas, L. A. 2011, *ApJ*, 726, 98
- Kirby, E. N., & Cohen, J. G. 2012, *AJ*, 144, 168
- Kirby, E. N., Guo, M., Zhang, A. J., et al. 2015a, *ApJ*, 801, 125
- Kirby, E. N., Simon, J. D., & Cohen, J. G. 2015b, *ApJ*, 810, 56
- Kobayashi, C., Umeda, H., Nomoto, K., Tominaga, N., & Ohkubo, T. 2006, *ApJ*, 653, 1145
- Kobayashi, C., Ishigaki, M. N., Tominaga, N., & Nomoto, K. 2014, *ApJ*, 785, L5
- Kobayashi, C., Karakas, A. I., & Lugaro, M. 2020, *ApJ*, 900, 179
- Koutsouridou, I., Salvadori, S., Skúladóttir, Á., et al. 2023, *MNRAS*, 525, 190
- Law, D. R., & Majewski, S. R. 2010, *ApJ*, 714, 229
- Layden, A. C., & Sarajedini, A. 2000, *AJ*, 119, 1760
- Lee, Y. S., Beers, T. C., Sivarani, T., et al. 2008a, *AJ*, 136, 2022
- Lee, Y. S., Beers, T. C., Sivarani, T., et al. 2008b, *AJ*, 136, 2050
- Lee, Y. S., Beers, T. C., Masseron, T., et al. 2013, *AJ*, 146, 132
- Limberg, G., Queiroz, A. B. A., Perottoni, H. D., et al. 2023, *ApJ*, 946, 66
- Limongi, M., & Chieffi, A. 2003, *ApJ*, 592, 404
- Limongi, M., & Chieffi, A. 2018, *ApJS*, 237, 13
- Lokas, E. L. 2024, *A&A*, 687, A82
- Longard, N., Jablonka, P., Arentsen, A., et al. 2022, *MNRAS*, 516, 2348
- Longard, N., Jablonka, P., Battaglia, G., et al. 2023, *MNRAS*, 525, 3086
- Lucchini, R., Lardo, C., Primas, F., et al. 2020, *A&A*, 644, A75
- Lucchini, R., Jablonka, P., Skúladóttir, Á., et al. 2024, *A&A*, 686, A266
- Lucey, M., Hawkins, K., Ness, M., et al. 2022, *MNRAS*, 509, 122
- Majewski, S. R., Skrutskie, M. F., Weinberg, M. D., & Ostheimer, J. C. 2003, *ApJ*, 599, 1082
- Martin, N. F., Starkenburg, E., Yuan, Z., et al. 2023, *A&A*, in press, <https://doi.org/10.1051/0004-6361/202347633>
- Mateo, M. L. 1998, *ARA&A*, 36, 435
- Matteucci, F. 2003, *Ap&SS*, 284, 539
- Mayer, L., Governato, F., Colpi, M., et al. 2001, *ApJ*, 547, L123
- McConnachie, A. W., & Venn, K. A. 2020, *AJ*, 160, 124
- McWilliam, A. 1997, *ARA&A*, 35, 503
- McWilliam, A., Wallerstein, G., & Mottini, M. 2013, *ApJ*, 778, 149
- Minelli, A., Bellazzini, M., Mucciarelli, A., et al. 2023, *A&A*, 669, A54
- Monaco, L., Bellazzini, M., Bonifacio, P., et al. 2005, *A&A*, 441, 141
- Mucciarelli, A., Bellazzini, M., Ibata, R., et al. 2017, *A&A*, 605, A46
- Norris, J. E., & Yong, D. 2019, *ApJ*, 879, 37
- Oh, W. S., Nordlander, T., Da Costa, G. S., Bessell, M. S., & Mackey, A. D. 2024, *MNRAS*, 528, 1065
- Oria, P.-A., Ibata, R., Ramos, P., Famaey, B., & Errani, R. 2022, *ApJ*, 932, L14
- Pace, A. B., Erkal, D., & Li, T. S. 2022, *ApJ*, 940, 136
- Pagnini, G., Salvadori, S., Rossi, M., et al. 2023, *MNRAS*, 521, 5699
- Peñarrubia, J., & Petersen, M. S. 2021, *MNRAS*, 508, L26
- Peñarrubia, J., Belokurov, V., Evans, N. W., et al. 2010, *MNRAS*, 408, L26
- Placco, V. M., Frebel, A., Beers, T. C., & Stancliffe, R. J. 2014, *ApJ*, 797, 21
- Revez, Y., & Jablonka, P. 2018, *A&A*, 616, A96
- Roederer, I. U., Karakas, A. I., Pignatari, M., & Herwig, F. 2016, *ApJ*, 821, 37
- Rossi, S., Beers, T. C., Sneden, C., et al. 2005, *AJ*, 130, 2804
- Ruiz-Lara, T., Gallart, C., Bernard, E. J., & Cassisi, S. 2020, *Nat. Astron.*, 4, 965
- Sánchez-Janssen, R., Méndez-Abreu, J., & Aguerri, J. A. L. 2010, *MNRAS*, 406, L65
- Santistevan, I. B., Wetzel, A., Sanderson, R. E., et al. 2021, *MNRAS*, 505, 921
- Sbordone, L., Bonifacio, P., Buonanno, R., et al. 2007, *A&A*, 465, 815
- Schiavon, R. P., Johnson, J. A., Frinchaboy, P. M., et al. 2017, *MNRAS*, 466, 1010
- Sestito, F., Buck, T., Starkenburg, E., et al. 2021, *MNRAS*, 500, 3750
- Sestito, F., Roediger, J., Navarro, J. F., et al. 2023a, *MNRAS*, 523, 123
- Sestito, F., Venn, K. A., Arentsen, A., et al. 2023b, *MNRAS*, 518, 4557
- Sestito, F., Zaremba, D., Venn, K. A., et al. 2023c, *MNRAS*, 525, 2875
- Sestito, F., Hayes, C. R., Venn, K. A., et al. 2024a, *MNRAS*, 528, 4838
- Sestito, F., Vitali, S., Jofre, P., et al. 2024b, *A&A*, 689, A201
- Siegel, M. H., Dotter, A., Majewski, S. R., et al. 2007, *ApJ*, 667, L57
- Simon, J. D., Jacobson, H. R., Frebel, A., et al. 2015, *ApJ*, 802, 93
- Skúladóttir, Á., Tolstoy, E., Salvadori, S., et al. 2015, *A&A*, 574, A129

- Skúladóttir, Á., Salvadori, S., Amarsi, A. M., et al. 2021, *ApJ*, **915**, L30
- Skúladóttir, Á., Puls, A. A., Amarsi, A. M., et al. 2023, *The Messenger*, **190**, 19
- Skúladóttir, Á., Koutsouridou, I., Vanni, I., et al. 2024a, *ApJ*, **968**, L23
- Skúladóttir, Á., Vanni, I., Salvadori, S., & Lucchesi, R. 2024b, *A&A*, **681**, A44
- Spencer, M. E., Mateo, M., Walker, M. G., et al. 2017, *AJ*, **153**, 254
- Stancliffe, R. J., Glebbeek, E., Izzard, R. G., & Pols, O. R. 2007, *A&A*, **464**, L57
- Starkenburg, E., Hill, V., Tolstoy, E., et al. 2013, *A&A*, **549**, A88
- Starkenburg, E., Martin, N., Youakim, K., et al. 2017, *MNRAS*, **471**, 2587
- Susmitha, A., Koch, A., & Sivarani, T. 2017, *A&A*, **606**, A112
- Tafelmeyer, M., Jablonka, P., Hill, V., et al. 2010, *A&A*, **524**, A58
- Taylor, M. B. 2005, in *Astronomical Society of the Pacific Conference Series*, 347, *Astronomical Data Analysis Software and Systems XIV*, eds. P. Shopbell, M. Britton, & R. Ebert, 29
- Tolstoy, E., Irwin, M. J., Helmi, A., et al. 2004, *ApJ*, **617**, L119
- Tolstoy, E., Skúladóttir, Á., Battaglia, G., et al. 2023, *A&A*, **675**, A49
- Umeda, H., & Nomoto, K. 2003, *Nature*, **422**, 871
- Vanni, I., Salvadori, S., Skúladóttir, Á., Rossi, M., & Koutsouridou, I. 2023, *MNRAS*, **526**, 2620
- Vasiliev, E., & Belokurov, V. 2020, *MNRAS*, **497**, 4162
- Venn, K. A., Irwin, M., Shetrone, M. D., et al. 2004, *AJ*, **128**, 1177
- Venn, K. A., Shetrone, M. D., Irwin, M. J., et al. 2012, *ApJ*, **751**, 102
- Vincenzo, F., & Kobayashi, C. 2018, *A&A*, **610**, L16
- Vitali, S., Arentsen, A., Starkenburg, E., et al. 2022, *MNRAS*, **517**, 6121
- Walker, M. G., & Peñarrubia, J. 2011, *ApJ*, **742**, 20
- Waller, F., Venn, K. A., Sestito, F., et al. 2023, *MNRAS*, **519**, 1349
- Wenger, M., Ochsenbein, F., Egret, D., et al. 2000, *A&AS*, **143**, 9
- Yang, Y., Hammer, F., Jiao, Y., & Pawlowski, M. S. 2022, *MNRAS*, **512**, 4171
- Yoon, J., Beers, T. C., Placco, V. M., et al. 2016, *ApJ*, **833**, 20
- Yoon, J., Whitten, D. D., Beers, T. C., et al. 2020, *ApJ*, **894**, 7
- Zhang, H.-X., Hunter, D. A., Elmegreen, B. G., Gao, Y., & Schruba, A. 2012, *AJ*, **143**, 47